AGU100 ADVANCING EARTH AND SPACE SCIENCE

JGR Solid Earth

RESEARCH ARTICLE
10.1029/2019JB017336

Key Points:
- We present high precision earthquake locations for ~70 years of instrumental seismicity in the Zagros fold-and-thrust belt of southern Iran
- We relocate ~2,500 earthquakes with epicentral uncertainties of <5 km, highlighting the existence of numerous unmapped faults
- Focal depth distribution (4–25 km) throughout the Zagros range implies earthquakes nucleate both within and beneath the sedimentary cover

Supporting Information:
- Supporting Information S1
- Table S1

Correspondence to:
E. Karasözen,
ezgikarasozen@gmail.com

Citation:
Karasözen E., Nissen, E., Bergman, E. A., & Ghods, A. (2019). Seismotectonics of the Zagros (Iran) from orogen-wide, calibrated earthquake relocations. *Journal of Geophysical Research: Solid Earth*, *124*, 9109–9129. https://doi.org/10.1029/2019JB017336

Received 10 JAN 2019
Accepted 13 JUL 2019
Accepted article online 22 JUL 2019
Published online 5 AUG 2019

Seismotectonics of the Zagros (Iran) From Orogen-Wide, Calibrated Earthquake Relocations

Ezgi Karasözen[1], Edwin Nissen[2], Eric A. Bergman[3], and Abdolreza Ghods[4]

[1]Department of Geophysics, Colorado School of Mines, Golden, CO, USA, [2]School of Earth and Ocean Sciences, University of Victoria, Victoria, British Columbia, Canada, [3]Global Seismological Services, Golden, CO, USA, [4]Department of Earth Sciences, Institute for Advanced Studies in Basic Sciences, Zanjan, Iran

Abstract We use calibrated earthquake relocations to reassess the distribution and kinematics of faulting in the Zagros range, southwestern Iran. This is among the most seismically active fold-and-thrust belts globally, but knowledge of its active faulting is hampered by large errors in reported epicenters and controversy over earthquake depths. Mapped coseismic surface faulting is extremely rare, with most seismicity occurring on blind reverse faults buried beneath or within a thick, folded sedimentary cover. Therefore, the distribution of earthquakes provides vital information about the location of active faulting at depth. Using an advanced multievent relocation technique, we relocate ~2,500 earthquakes across the Zagros mountains spanning the ~70-year instrumental record. Relocated events have epicentral uncertainties of 2–5 km; for ~1,100 of them we also constrain origin time and focal depth, often to better than 5 km. Much of the apparently diffuse catalog seismicity now collapses into discrete trends highlighting major active faults. This reveals several zones of unmapped faulting, including possible conjugate left-lateral faults in the central Zagros. It also confirms the activity of faults mapped previously on the basis of geomorphology, including oblique (dextral-normal) faulting in the NW Zagros. We observe a primary difference between the Lurestan arc, where seismicity is focused close to the topographic range front, and the Fars arc, where out-of-sequence thrusting is evident over a width of ~100–200 km. We establish a focal depth range of 4–25 km, confirming earlier suggestions that earthquakes are restricted to the upper crust but nucleate both within and beneath the sedimentary cover.

1. Introduction

The Zagros mountains of southwestern Iran are one of the most rapidly deforming and seismically active fold-and-thrust belts on Earth, with abundant earthquakes of up to M_w 7.3 (Figure 1). Within the most seismically active, lower-elevation part of the range—known as the Simply Folded Belt (SFB)—folding of sedimentary rocks is expressed at the surface by series of anticlines and synclines which dominate the range physiography. Mapped surface faulting associated with earthquakes is extremely rare, with most seismicity occurring on blind reverse faults buried beneath or within a ~7- to 14-km-thick sedimentary cover. Therefore, the distribution of earthquakes provides the most accessible information about the location of active faulting at depth.

One means of mapping active faulting more comprehensively would be to determine accurate locations of moderate- to large-magnitude earthquakes, which should align along the major seismogenic structures. Unfortunately, epicenter catalog uncertainties that routinely exceed 10–20 km can easily lead to misidentification of the responsible faulting even for large earthquakes with source dimensions of tens of kilometers (Engdahl et al., 2006). Some earthquakes in Iran are mislocated by significantly larger distances, due in part to the lack of local seismic data; catalog errors for some older events are even known to exceed ~100 km (Berberian, 1979). Accurate earthquake depths are equally invaluable for understanding the tectonics of this mountain belt, yet catalog depths are often insufficient for these purposes. The Global Centroid Moment Tensor (GCMT) database calculates centroid solutions from low-pass-filtered body and surface waves, but centroid depths for upper crustal earthquakes are often held fixed due to instabilities in the inversion (Dziewonski et al., 1981; Ekström, 1989; Ekström et al., 2012; Konstantinou & Rontogianni, 2011). The International Seismological Centre (ISC) and the National Earthquake Information Center (NEIC) focal depths rely almost entirely on *P* wave arrival times and therefore suffer from the trade-off between origin time and depth, leading to errors of several tens of kilometers (Engdahl et al., 2006; Jackson, 1980; Maggi et al., 2002).

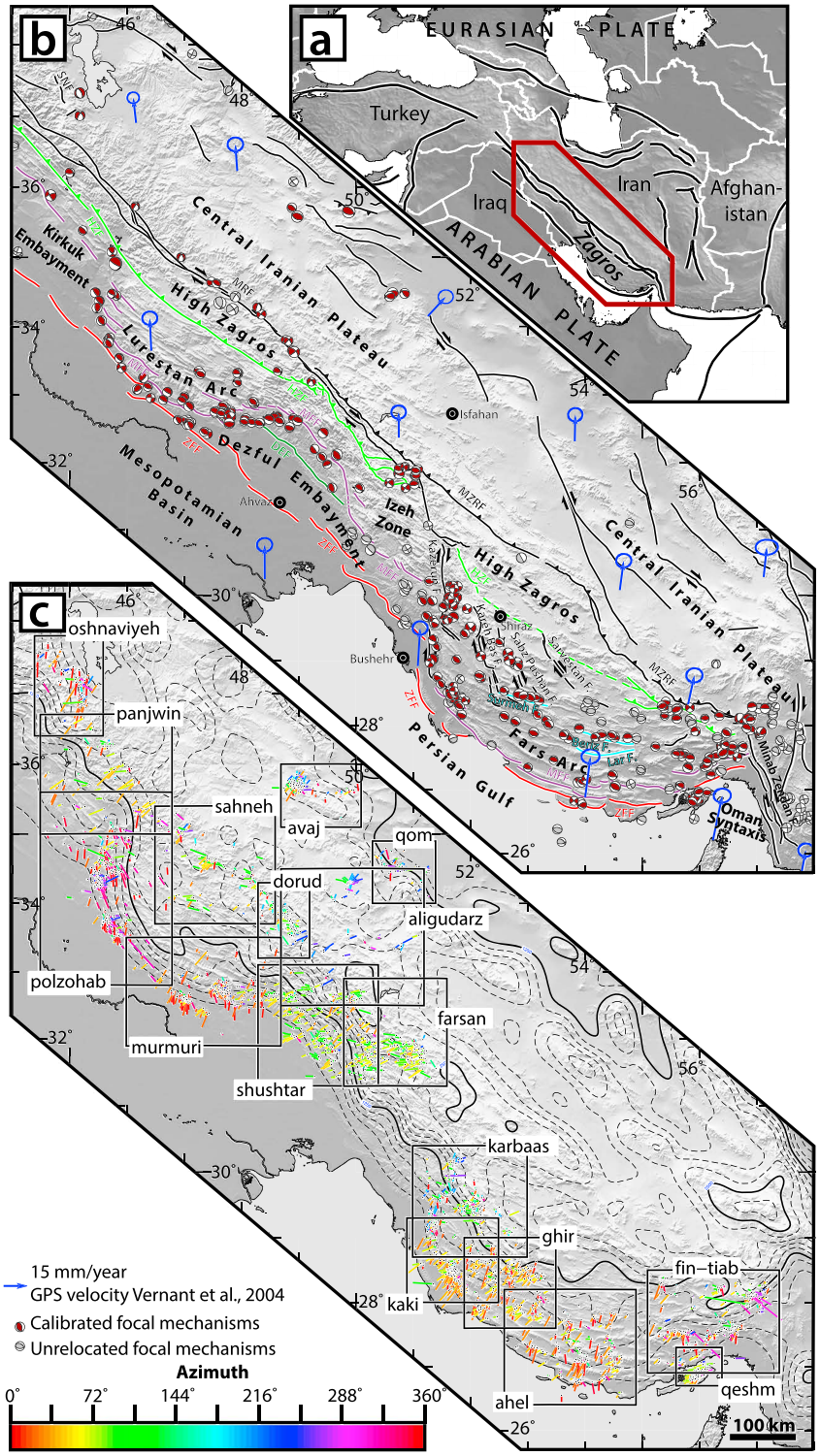

Figure 1. (a) Location of the Zagros within the Arabia-Eurasia collision zone. (b) Major surface-breaking faults are in black and Berberian's (1995) "master blind thrusts" are in color. DEF = Dezful embayment Fault; HZF = High Zagros Fault; MFF = Mountain Front Fault; MRF = Main Recent Fault; MZRF = Main Zagros Reverse Fault; ZFF = Zagros Foredeep Fault, SNF = Serow Normal Faults (Copley & Jackson, 2006). Focal mechanisms calibrated in this study are shown in red, and focal mechanisms that we were unable to relocate are in gray. GPS velocities relative to stable Eurasia are shown in blue with 1σ confidence ellipses (Vernant et al., 2004). (c) Colored vectors show the shifts from initial International Seismological Centre locations to final calibrated locations (black dots), color coded by azimuth. Black rectangles show the locations of individual clusters. Topography is contoured at 250 m intervals with the 1,250-m contour highlighted in bold.

The Engdahl, van der Hilst, and Buland (EHB) catalog of Engdahl et al. (1998) significantly improves focal depth resolution by incorporating teleseismic depth phases *pP* and *sP*, but these are difficult to pick for upper crustal events since the *pP–P* and *sP–P* delays are short (e.g., <5 s). This leads to errors of ~10 km which can mask important regional variations in belts of mostly shallow seismicity like the Zagros (Maggi et al., 2000). In such regions, the most accurate centroid depths are provided by independent teleseismic body waveform modeling studies and yield typical uncertainties of ±4 km (e.g., Engdahl et al., 2006; Maggi et al., 2000; Nissen et al., 2014; Talebian & Jackson, 2004). However, such analyses are not yet routine and can only be applied to events larger than $M_w \sim 5$–5.5. Recent studies show that regional moment tensors can constrain centroid depths for events larger than $M_w \sim 3$–3.5, with errors of 2–4 km (e.g., Ghods et al., 2012; Donner et al., 2013, 2014), but these analyses require a good station distribution at regional distances.

Berberian (1995) first suggested that seismic activity in the Zagros is concentrated on a small number of large, steeply dipping, basement-cored faults—termed "master blind thrusts"—that pass upward into the lower sedimentary cover where they control observed steps in exposed stratigraphic level. Berberian (1995) noticed that certain anticlines in the SFB accommodate large steps of up to a few kilometers in stratigraphic level, with exposures of younger strata on the southern/southwestern side of the fold in the footwall and older strata to the east/northeast in the hangingwall. He attributed these abrupt changes in stratigraphic level and asymmetric fold shapes to the presence of discrete reverse faults in the underlying basement. A key tenet of Berberian's (1995) hypothesis is that most large, early instrumental earthquakes in the Zagros can be attributed to one of these discrete structures. This model has prevailed for more than 20 years, despite large uncertainties in the catalog earthquake locations upon which it is partly based. The veracity of Berberian's (1995) model has obvious implications for the treatment of seismic hazard in the Zagros. It also has important repercussions for our understanding of fold-and-thrust structural relations, because it implies that away from the master blind thrusts, anticlines are not cored by reverse faults, as some other structural models have suggested (e.g., Allen et al., 2013; McQuarrie, 2004).

In this paper we test Berberian's (1995) hypothesis by relocating the ~70-year back-catalog of instrumentally recorded earthquakes across the Zagros. Though the relocation procedure we employ has been used before within the Zagros for targeted aftershock studies (e.g., Copley et al., 2015; Ghods et al., 2012), applying it across an entire orogen and to several decades of seismic data is unprecedented, and only made possible by significant recent (~2005 onward) improvements in station coverage. The resulting minimally biased locations help us investigate whether seismicity is localized along large basement faults, in agreement with Berberian (1995), or distributed more diffusely among shallow faults and folds as some newer studies have proposed (e.g., Allen et al., 2013; McQuarrie, 2004). A related test is whether earthquake faulting is concentrated within the outermost part of the SFB, as has been suggested on the basis of sparse campaign GPS measurements (Walpersdorf et al., 2006), or whether many interior parts of the Zagros are also still seismically active (Walker et al., 2005). Finally, with minimally biased depth resolution now possible for many newer events, we provide new estimates of the seismogenic depth range which helps distinguish the relative importance of basement and cover faulting (e.g., Barnhart & Lohman, 2013; Nissen et al., 2011, 2014).

2. Tectonic Background

The Zagros mountains are a major element within the southern Alpine-Himalayan orogen, extending from the Turkish border southeastward for ~1,600 km to the Gulf of Oman (Figures 1a and 1b). They comprise one of the youngest continental collision zones globally, produced by the collision between Arabia and central Iran following northward subduction of the Neotethys ocean, with an inferred late Eocene onset of shortening and a dated Miocene onset of folding in the outer SFB (e.g., Ballato et al., 2008; Guest et al., 2007; Morley et al., 2009; Vergés et al., 2019). The Zagros currently accommodates almost half of the present-day shortening between Arabia and Eurasia (Vernant et al., 2004), but both the style and rate of deformation differ along strike of the range. Faster GPS velocities (~9 mm/year relative to central Iran) are observed in the southeastern Zagros, where convergence is perpendicular to the range and accommodated by pure shortening (Vernant et al., 2004; Walpersdorf et al., 2006). As the trend of the range changes from E-W to NW-SE in the central and northwestern Zagros, GPS velocities decrease to ~4 mm/year relative to central Iran, and convergence obliquity is partitioned into shortening on range-parallel thrusts and dextral shear along the NW-SE trending Main Recent Fault (Authemayou et al., 2009; Talebian & Jackson, 2004; Figures 1b and 2). Seismic deformation rates calculated from ~100 years of seismicity account for around half of the geodetic (GPS-derived) shortening rate in the northwestern Zagros and for less than one third of the geodetic rate in

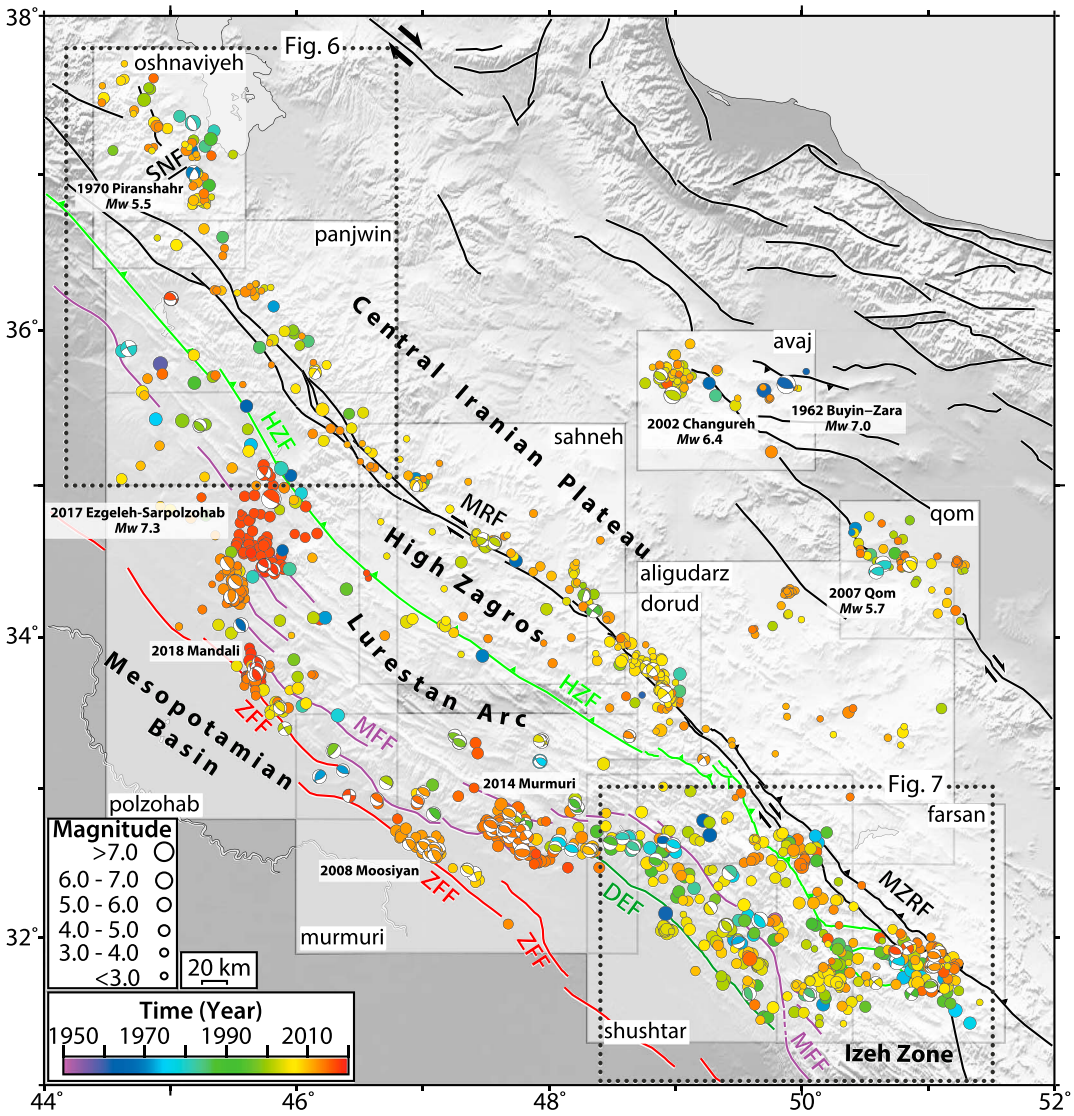

Figure 2. Calibrated epicentral locations in the northwestern Zagros and adjacent central Iranian plateau, colored by time and scaled by magnitude. Where they are available (from the references listed in Table S2), teleseismic focal mechanisms are plotted at their relocated epicenters using the same scaling and coloring. White shaded regions show the extent of individual clusters as in Figure 1c. Major surface-breaking faults are in black and Berberian's (1995) "master blind thrusts" are in color. DEF = Dezful embayment Fault; HZF = High Zagros Fault; MFF = Mountain Front Fault; MRF = Main Recent Fault; MZRF = Main Zagros Reverse Fault; ZFF = Zagros Foredeep Fault, SNF = Serow Normal Faults.

the southeastern Zagros (Barnhart et al., 2013; Jackson & McKenzie, 1984; Masson et al., 2005; Palano et al., 2017). The shortfall is likely accounted for by a mixture of folding, aseismic fault creep (e.g., Barnhart et al., 2013), and ductile shortening of the basement (Allen et al., 2013; Nissen et al., 2011).

An abrupt cutoff between the intense seismicity of the Zagros and the quiescent central Iranian plateau occurs along the NW-SE trending Main Zagros Reverse Fault (Figure 1b). This major geological boundary separates the metamorphic and volcanic rocks of central Iran to the NE from the deformed Arabian continental margin sediments to the SW (e.g., Berberian & King, 1981), but it appears mostly inactive. The Zagros itself is often divided into two structurally and tectonically distinct domains (Figures 1b, 2, and 3): (1) The High Zagros is a zone of high topography (maximum elevations of ~4,000 m), features steep, NE dipping, surface-breaking reverse faults and exposes older and more deformed Arabian plate rocks (Authemayou et al., 2009; Berberian, 1995; Falcon, 1974; Talebian & Jackson, 2004); (2) the SFB is lower in elevation and characterized by long (up to ~200 km), parallel arrays of anticlines and synclines, mostly concentric in shape

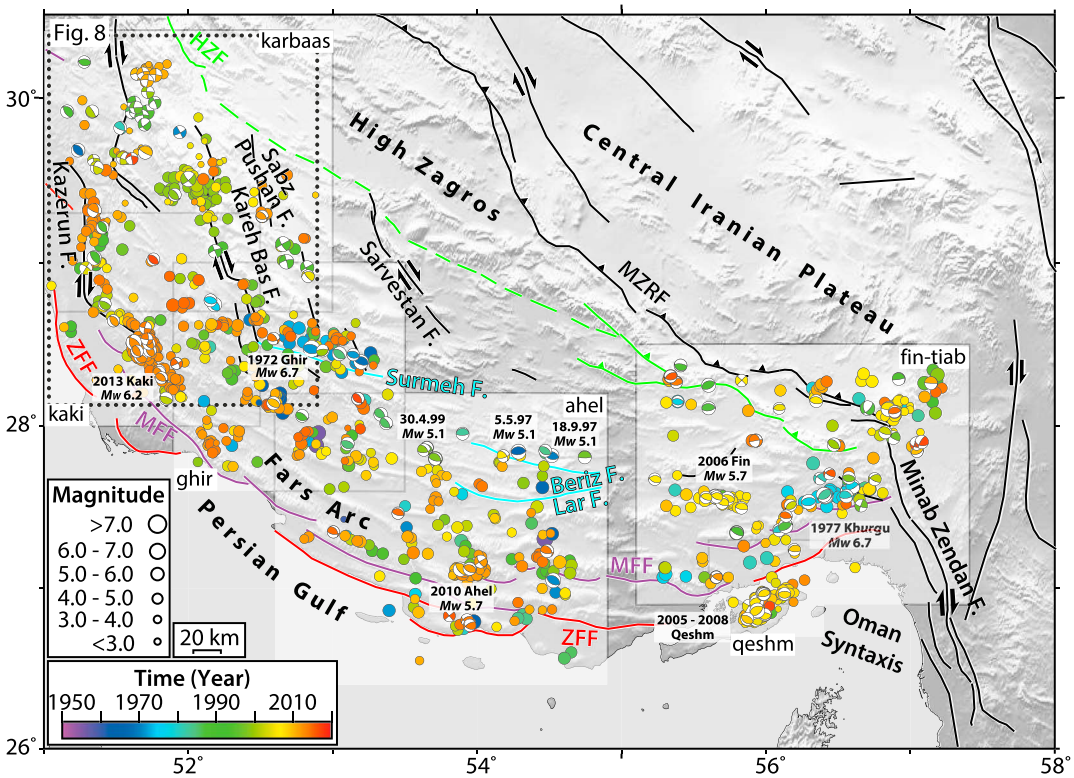

Figure 3. Calibrated epicentral locations in the southeastern Zagros, colored by time and scaled by magnitude. Where they are available (from the references listed in Table S2), teleseismic focal mechanisms are plotted at their relocated epicenters using the same scaling and coloring. White shaded regions show the extent of individual clusters as in Figure 1c. Major surface-breaking faults are in black and Berberian's (1995) "master blind thrusts" are in color. HZF = High Zagros Fault; MFF = Mountain Front Fault; MZRF = Main Zagros Reverse Fault; ZFF = Zagros Foredeep Fault.

(though some verge toward the SW) and with typical half-wavelengths of ~10 km. The NW striking High Zagros Fault marks the boundary between these two structurally distinct domains and is associated with the only record of cosesimic surface rupture in the Zagros, in the 6 November 1990 M_w 6.4 Furg earthquake (Walker et al., 2005; Figure 1b). The SFB is further subdivided along strike into the higher elevation Lurestan arc, Izeh zone, and Fars arc, and the lower elevation Kirkuk embayment, Dezful embayment, and Oman syntaxis.

2.1. Stratigraphy, Geology, and Structure

The Zagros hosts the most productive reservoir rocks in the world, prompting interest in its subsurface structure and stratigraphy. According to offshore seismic reflection profiles in the central and eastern Persian Gulf, the total (undeformed, unexumed) cover thickness is ~12–16 km (Jahani et al., 2009; Jahani et al., 2017), while balanced cross sections in the foreland of the northwestern Zagros show cover thicknesses there of ~11–14 km (e.g., Blanc et al., 2003; Casciello et al., 2009; Vergés et al., 2011). These values are somewhat greater than cover thicknesses from balanced cross sections across the SFB itself, which range from ~6–10 km in the Lurestan arc (e.g., Blanc et al., 2003; Farzipour-Saein et al., 2009; Homke et al., 2009; McQuarrie, 2004; Vergés et al., 2011) to ~9–15 km in the Dezful embayment and Fars arc (e.g., Ahmadhadi et al., 2007; Blanc et al., 2003; Derikvand et al., 2018; Sherkati et al., 2006). These estimates are based on geological interpretations and as their wide ranges suggest, the basement depth is not resolved well for thicknesses >10 km. Estimates are further hampered by the presence of salt formations which do not allow seismic waves to penetrate to greater depths. Teknik & Ghods's (2017) fractal spectral analysis of aeromagnetic data revealed that the depth of magnetic basement is 7–16 km in the Zagros and that the sedimentary thickness is ~5 km shallower in the High Zagros than in the SFB. The cover thickness NE of the High Zagros Fault is reduced significantly, with its exact value varying substantially according to location and interpretation.

In the southeastern Zagros, the basement is detached from the sedimentary cover by the weak Infracambrian Hormuz Formation, an interbedded succession of evaporites and other deposits which are brought to the surface by numerous salt diapirs (Jahani et al., 2007; Kent, 1970). Hormuz salt outcrops across much of the Fars arc and there may be an equivalently weak layer within the north west, based on similarities in folding patterns (e.g., Carruba et al., 2006; Sherkati & Letouzey, 2004). It is overlain by the "Competent Group" (O'Brien, 1957), a succession of platform carbonates and clastic rocks that behave structurally as a single, thick unit. Above, the middle cover comprises more limestones, interbedded with weaker marls, shales, and evaporites, that together include important hydrocarbon sources, cap rocks, and reservoirs (e.g., the Asmari limestone). The sequence is capped by up to ~4 km of Miocene-Recent sandstones and conglomerates, marking the onset of continental collision, uplift and erosion (Fakhari et al., 2008; Hessami et al., 2001; Khadivi et al., 2010).

Structural relations between folding and faulting, and their relative importance in accommodating overall shortening, are complicated by the potential decoupling of the basement from the sedimentary cover by the numerous ductile layers. Balanced cross sections across the Zagros are in good agreement over the total amount of shortening—50–80 km according to most estimates—but disagree markedly over how it is achieved (e.g., Vergés et al., 2011). Early models invoked buckling (detachment folding) of the sedimentary cover over a single décollement in the Hormuz salt, with faulting and seismicity assumed to be restricted to the underlying basement (e.g. Colman-Sadd, 1978; Falcon, 1969; Stöcklin, 1968). More recently, it has emerged that parts of the Zagros—particularly within the Lurestan arc and Dezful embayment—contain additional, shallower detachment levels which control regional variations in fold styles and wavelengths (Carruba et al., 2006; Casciello et al., 2009; Vergés et al., 2011). In addition, it is now recognized that many large earthquakes occur within competent units of the middle-to-lower sedimentary cover (Copley et al., 2015; Elliott et al., 2015; Nissen et al., 2007, 2011, 2014), linked to surface anticlines through a mixture of fault propagation, fault bend, and detachment folding.

2.1.1. Berberian's (1995) "Master Blind Thrusts"

Berberian (1995) mapped a few distinct structural and topographic steps across which large, vertical changes (up to few kilometers) in exposed stratigraphy are accommodated (colored lines, Figure 1b). He hypothesized that these correspond to high-angle reverse faults—master blind thrusts—that nucleate in the basement and break upward into the sedimentary cover. These proposed faults were considered responsible for numerous moderate magnitude ($M_w \sim 5$–6) and two larger (1972 M_w 6.7 Ghir and 1977 M_w 6.7 Khurgu) historical and early instrumental earthquakes.

Among Berberian's (1995) master blind thrusts (Figures 1b, 2, and 3), the High Zagros Fault is the only known (rather than inferred) surface-breaking fault. Its southeastern section appears to be most seismically active, hosting the surface-rupturing 1990 M_w 6.4 Furg earthquake (Walker et al., 2005). Two more of Berberian's (1995) inferred that faults can be traced across the entire length of the range, albeit discontinuously: the Zagros Foredeep Fault which follows subdued frontal folds, and behind it the Mountain Front Fault which marks the regional southern limit of Asmari limestone outcrops and thus the major topographic rangefront. Berberian (1995) associates the Zagros Foredeep Fault with several $M \sim 5$–6 earthquakes and with one historical $M \sim 6.5$ earthquake in 840 CE, and the Mountain Front Fault with the 1977 M_w 6.7 Khurgu earthquake, a historical event of $M \sim 6.8$ in 1052 CE, as well as several smaller instrumental and historical earthquakes.

The other inferred master blind thrusts are significantly shorter, each being restricted to a single tectonic domain (arc or embayment; Figure 1b). The Dezful Embayment Fault is regionally another major rangefront-forming fault, analogous to the Mountain Front Fault in other parts of the Zagros; Berberian (1995) links it with M_w 6.1 and 5.3 thrust earthquakes in 1977 and 1985, respectively (Figure 2). In the northern Fars arc, the Surmeh fault is associated with six destructive earthquakes, with the 1972 M_w 6.7 Ghir earthquake being the largest (Figure 3). In the central Fars arc, the Lar and Beriz-Dehkuyeh faults follow E-W trends in Hormoz Salt domes and, according to Berberian (1995), hosted M_s 5.7–6.5 earthquakes in the 1960s (Figure 3). Berberian (1995) does not extend his analysis into the Kirkuk embayment in the northwesternmost Zagros (Iraqi Kurdistan).

However, the assumed locations of these earthquakes are based either on felt reports which are highly unreliable (Berberian, 1979, 1981) or on early teleseismic epicenters which have large uncertainties. In addition, there has never been a permanent seismic network in the Zagros and the earthquake catalog epicenters used

by Berberian (1995) were determined in single-event analyses using arrival times at distant Global Digital Seismic Network stations. We now know that in the Zagros, epicenters determined in this way—such as those listed in the widely used GCMT, ISC, and NEIC catalogs—may be mislocated by as much as 50–60 km, as revealed by coseismic surface deformation mapped with InSAR (Barnhart et al., 2013). These mislocations reflect both scatter and bias introduced by seismic velocity perturbations in regions surrounding the Zagros which are not accounted for in standard whole Earth velocity models. Errors of this magnitude are somewhat larger than those typical of continental regions (Weston et al., 2011), though similar uncertainties are observed in the Andes (Devlin et al., 2012). Clearly, such errors prevent a confident association of any single earthquake in the Zagros with Berberian's (1995) master blind thrusts, or any other individual fault, except for those few recent earthquakes mapped with InSAR. Although Berberian's (1995) interpretation is still the most widely accepted structural model for faulting in the Zagros (e.g., Blanc et al., 2003; Mouthereau et al., 2007; Sherkati et al., 2006; Talebian & Jackson, 2004), there are alternatives that support more distributed faulting, some of which do not require faults to nucleate within the basement at all (e.g., Alavi, 2007; Carruba et al., 2006; McQuarrie, 2004).

2.1.2. Strike-Slip Faulting

Strike-slip faulting is important in two parts of the Zagros. First, in the northwestern High Zagros the right-lateral, NW-SE striking Main Recent Fault follows the main trace of the Main Zagros Reverse Fault west of ~51°E, becoming more and more distinct toward the northwest (Ricou et al., 1977; Talebian & Jackson, 2002; Tchalenko & Braud, 1974; Figures 1b and 2). This fault likely accommodates most of the partitioned, range-parallel dextral shear at these longitudes (Authemayou et al., 2009; Vernant et al., 2004; Walpersdorf et al., 2006). The Main Recent Fault and its splays account for many of the largest earthquakes in the Zagros, including the 1909 M_s 7.4 Silakhor, 1957 M_w 6.7 Farsinaj, 1958 M_w 6.7 Firuzabad, and 2006 M_w 6.1 Silakhour earthquakes (Ambraseys & Melville, 1982; Ambraseys & Moinfar, 1973; Berberian, 2014; Berberian & Yeats, 2001; Ghods et al., 2012) and likely accommodate ~2–12.5 mm/year of dextral motion (Authemayou et al., 2009; Vernant et al., 2004; Walpersdorf et al., 2006).

Second, in the western Fars arc, a series of N-S trending, right-lateral faults have been mapped on the basis of earthquake focal mechanisms and offsets and deflections of fold axes (Ricou, 1974; Baker et al., 1993; Hessami et al., 2001; Authemayou et al., 2006; Figures 1b and 3). These faults may accommodate along-strike extension of the central Zagros by rotating about vertical axes through time (Talebian & Jackson, 2004). The largest is the Kazerun fault which has a likely slip rate of ~2–6 mm/year (Authemayou et al., 2009; Berberian & King, 1981; Berberian, 1995; Tavakoli et al., 2008; Walpersdorf et al., 2006) and consists of four N-S trending, right-stepping segments with the central segment being the most active in both historical (intensity >XIII) and instrumental (magnitude ~5–6) seismicity (Ambraseys & Melville, 1982; Baker et al., 1993; Berberian, 1995; Berberian & Tchalenko, 1976; Sepehr & Cosgrove, 2005; Talebian & Jackson, 2004). Geological mapping suggests that the Kazerun fault limits the distribution of Hormuz salt to the west and thus exerts an influence on regional variations in structure style, the distribution of deformation, and sedimentary thickness (Sepehr & Cosgrove, 2005).

Further east (Figures 1b and 3), the Kareh Bas fault is linked by Berberian (1995) with the 1992 M_b 5.2 Dadenjan earthquake, and the Sabz-Pushan fault may have hosted two M_w 5.6 and 5.8 events in 1985 and 1987 (Baker, 1993; Maggi et al., 2000). Berberian (1995) also links two M 6.4 historical events in 1824 CE and 1890 CE with the Sabz-Pushan fault (Ambraseys & Melville, 1982). Further east still, the Sarvestan fault has little clear record of instrumental seismicity.

Though all of the central Zagros strike-slip faults exhibit some geomorphological expression, none of them are linked with surface-rupturing earthquakes. Instead, any association with instrumental events is based on epicenters, which may have large uncertainties.

2.2. Seismicity

Away from the main strike-slip faults, most earthquakes in the Zagros exhibit reverse focal mechanisms with moderately dipping (30–60°) nodal planes that may reflect the reactivation of normal faults inherited from the stretched passive margin of Arabia (Jackson, 1980) (Figure 1b). There are a large number of earthquakes of up to $M_w \sim 6.5$, with only a handful of larger events including just two larger than M_w 7 (the 23 January 1909 M_s 7.4 Silakhor and 12 November 2017 M_w 7.3 Ezgeleh-Sarpolzahab earthquakes). The historical record also apparently lacks earthquakes larger than about M 7, despite being fairly reliable as far back as the seventh century CE (Ambraseys & Melville, 1982).

Since mapped surface rupturing is extremely rare—and absent altogether within the SFB even for the largest modern events (Ghir, Khurgu, Ezgeleh-Sarpolzahab)—earthquakes were for a long time assumed to occur mostly or even exclusively, within the basement (e.g.. Berberian, 1981; Jackson & Fitch, 1981; Ni & Barazangi, 1986; Talebian & Jackson, 2004). Support for this view was also provided by the first microseismic experiments in the Zagros, which showed concentrations of smaller earthquakes at probable basement depths (Hatzfeld et al., 2003; Tatar et al., 2004). However, work published within the past few years has challenged this consensus. Early InSAR studies of Lohman and Simons (2005) and Nissen et al. (2007) first showed conclusively that several moderate-sized thrust earthquakes in the Fars arc had occurred within the sedimentary cover. In light of these results, Nissen et al. (2011) reassessed the many earlier teleseismic body waveform modeling results to suggest that the majority of the larger earthquakes, with typical centroid depths of ∼5–10 km, are centered within the cover. While subsequent work by Barnhart and Lohman (2013) suggested that some of these events may trigger shallow aseismic fault creep, joint seismo-geodetic analyses have since confirmed rupture entirely within the cover in a few earthquakes (Nissen et al., 2014; Copley et al., 2015; Elliott et al., 2015). However, the relatively small number of earthquakes mapped with InSAR (compared to those recorded teleseismically) means that geodetic studies alone offer a limited test of Berberian's (1995) hypothesis.

3. Calibrated Earthquake Locations

We reanalyze the ∼70-year back-catalog of instrumentally recorded seismicity in the Zagros using the *mloc* multiple-earthquake relocation technique that has been specialized for studies of absolute, calibrated locations (Bergman & Solomon, 1990; Karasözen et al., 2018; Walker et al., 2011). *Mloc* is based on the hypocentroidal decomposition (HD) algorithm of Jordan and Sverdrup (1981) that seeks to minimize the location bias arising from unknown Earth velocity structure. This technique has been applied to several individual earthquake sequences in the Zagros and elsewhere in Iran (e.g., Aziz Zanjani et al., 2013; Elliott et al., 2015; Ghods et al., 2012; Nissen et al., 2010; Walker et al., 2011) but never before to seismicity across an entire orogen. Early instrumental events can be relocated if there is enough connectivity between them and modern events in the cluster; preferably, at least ∼10 shared readings from the same stations (e.g., Karasözen et al., 2016; Walker et al., 2011).

The largest contribution to the uncertainty in hypocenter locations comes from unknown Earth velocity structure. Well-established *relative* multiple-earthquake relocation techniques, including *mloc*, minimize these errors by correlating traveltime errors along similar paths. Since the ray paths from closely clustered group of earthquakes sample the same portion of the Earth, traveltime differences mostly account for relative hypocenter locations. However, in order to match seismicity with causative faulting it is vital to obtain *calibrated* locations, defined as *absolute* locations accompanied by realistic estimates of uncertainties. The key to doing so with *mloc* lies in the HD algorithm, which divides the earthquake relocation into two independent inverse problems and enables the data set to be tailored to each step. First, it solves for the *cluster vectors* which link each event to the geometric mean of all hypocenters in the cluster, the *hypocentroid*. At this relative location step, all available data at any epicentral distance can be used.

Second, it calculates the absolute location of the hypocentroid and updates the absolute coordinate of every event in the cluster. This step is critical because whether a cluster can be called as calibrated or not depends heavily on a minimally biased hypocentroid. Here, the type and quality of available data defines one of two types of calibration strategy. (1) In the *direct calibration* mode, data at close-in distances (distances < Pg/Pn and Sg/Sn crossover) are preferred since modeling direct arrival phases (Pg and Sg) with shorter path lengths would minimize the biasing effect of unknown velocity structure. The distance limit for the hypocentroid estimation depends on the availability of close-in data and its completeness of azimuthal coverage. (2) The alternative *indirect calibration* mode takes advantage of the ground truth locations of one or more events in the cluster determined by other independent means and then shifts the entire cluster in space and time to match to this known location.

Our goal is to calibrate all four parameters of the hypocenter(s): latitude, longitude, focal depth, and origin time. The last two are most challenging since they trade off with each other, and their resolution depends on the accuracy of the velocity model and the availability of depth-sensitive phases. Depth phase (pP, sP, sS) arrival times are useful for deeper teleseismic events but are usually insufficient for shallower earthquakes due to the difficulties in phase identification. Near-source (distances <2 times the focal depth) direct Pg and

Sg waves, if observed, can provide strong constraints for local events up to distances of several (~1.5–2.0) times the focal depth; at larger distances, the traveltime derivatives lose sensitivity to depth (e.g., Havskov & Ottemoller, 2010). In cases like this, the HD method can solve depth as a free parameter and provide <3 km uncertainties. However, if one or more events in a cluster are too unstable for free depth solutions—often due to bad picks at nearby stations—solving for depth can cause convergence problems, and it becomes preferable to fix the depths of individual events manually by minimizing the residuals at close-in stations. In these situations, the uncertainty estimation varies according to which arrival time data are employed for the focal depth calculation: 2–3 km where near-distance data are utilized, 3–4 km where local-distance data (distances >2 times the focal depth and < *Pg*/*Pn* crossover) are utilized, and 4 km where depth phases are used. These estimates are based on our experience assessing the fit between observed phase arrivals and theoretical traveltimes at close-in distances across several clusters. If there are insufficient data to estimate depth, then events are fixed to a cluster default value that minimizes the trade-off between the available arrival times and the predicted traveltimes (Karasözen et al., 2016).

In this study, we expand our depth analysis by developing a new routine that exploits both near-source direct arrivals and more distant refracted phases (Figure S1 in the supporting information). We first start with a set of *control events* that have one or more direct phase picks at short epicentral distances (ideally < 1.0°) with a good azimuthal coverage (<180°) and depth control (*Pg*, *Sg*, $S - P$ picks from near-distance stations). These control events are placed in a subcluster, first, to constrain the focal depths using *Pg* and *Sg* phases at near-distances and, second, to refine the local crustal and upper mantle velocity model using *Pn* and *Sn* arrival times. Once the control event depths and velocity model are established, then noncontrol events (those with few *Pg*, *Sg* readings at local-distances) can be added to the cluster. At this stage, we take advantage of two relations: (1) the origin time of a noncontrol event will be driven by the fit of its *Pn* readings, due to their steep take-off angles, to those of the control events; and (2) the *Pg* arrivals at regional distances are insensitive to changes in focal depth, but are affected by changes in origin time. For example, if the assumed depth of a noncontrol event is greater than its true depth, then the residual of its *Pg* reading will be negative because its origin time must be later to fit its *Pn* arrivals with shorter ray paths. With this new procedure, and by exploiting recent improvements in local arrival time data, we can reduce uncertainties in focal depths to ~4 km or better for well-recorded events.

The improved two-step HD analysis in *mloc* usually converges to a stable solution in 2–4 iterations, and each run is followed by a cleaning process where outlier readings are identified and removed iteratively. *Mloc* analyzes multiple repeated arrival time data in a cluster (i.e., the same station-phase pairs from different events) and uses the spread of these picks (Croux & Rousseeuw, 1992) to determine empirical reading errors. These errors are then used both to weight the arrival time data in the inversion and to identify outliers. This weighting scheme does not include any specific weighting for individual phases but is instead based on the spread of the station-phase pairs from every event in the cluster. After each run, outliers are removed iteratively until there are no readings with residuals greater than 3 sigma. The resulting data set approximately resembles a Gaussian distribution encompassing the traditional picking errors and any additional source of error, leading to a rigorous characterization of location uncertainty.

The *mloc*'s phase identification algorithm works differently for each inversion step. For the close-in distances at which the hypocentroid is calculated, all phases are forced to be either *Pg* or *Sg* and are flagged if they cannot be labeled. For the distances where cluster vectors are calculated (i.e., regional and teleseismic distances), the closest pick to the theoretical traveltime is selected as the phase label. The accuracy of regional and teleseismic phase labeling is not as important as these phases are only used to calculate relative locations. The most challenging phase labeling occurs at the *Pg*/*Pn* and *Sg*/*Sn* crossover; although *mloc* automatically relabels picks at these distances, we analyze these in more detail by carefully assessing the residuals.

3.1. Application to the Zagros

Our Zagros clusters are focused in areas containing well-recorded recent earthquakes. Each cluster can have at most 200 events; *mloc* is ill-suited for larger numbers due to the higher computational demands of singular value decomposition required for the inversion. We focus the makeup of each cluster on larger events and their aftershock sequences—especially those with published focal mechanisms from several first motions or body waveform modeling studies or from the GCMT catalog (Table S2)—so long as they are sufficiently well-recorded (>15 readings, azimuthal gap <180°). Cluster dimensions are also limited to ~200 km; from

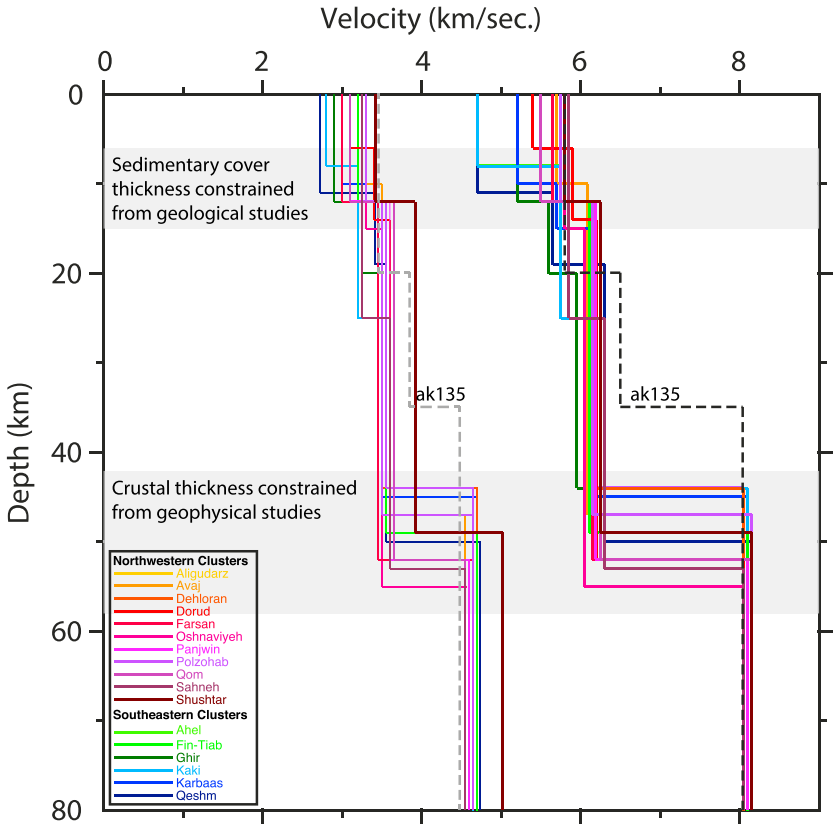

Figure 4. Individual 1-D custom crustal *P* wave (right) and *S* wave (left) velocity models obtained for each cluster in this study. Each cluster is specified with different colors: northwestern clusters are color coded with yellow-red-purple shades, and southeastern clusters are color coded with green-blue shades. The *ak*135 velocity model (shown with dashed line) is used for all noncrustal phases at distances >17° (Kennett et al., 1995). Estimates for the thickness of the basement is taken from McQuarrie (2004), Molinaro et al. (2005), Mouthereau et al. (2007), Oveisi et al. (2009), Allen et al. (2013), Blanc et al. (2003), Sherkati et al. (2005), Abdollahie-Fard et al. (2006), and Casciello et al. (2009), and for the thickness of the crust from Hatzfeld et al. (2003), Afsari et al. (2011) and Tatar and Nasrabadi (2013).

our experience working in complex tectonic settings like the Zagros, at larger distances the hypocentroid is prone to biases arising from lateral velocity heterogeneities. A few of our clusters are colocated with ones published previously, but in these instances we are able to improve epicentral and focal depth constraints and extend the analysis in time by incorporating new data. Our priority is to generate robust calibrated epicenters where feasible, rather than trying to relocate every last event, and so our clusters are naturally concentrated in areas with good local station coverage and active seismicity. Consequently, our relocated seismicity maps should be interpreted more as indicating where earthquakes *have* occurred than where they have *not*. Significant gaps where we were unable to calibrate any seismicity include (1) the southern Dezful embayment between the Farsan and Karbaas clusters, (2) the central interior Fars arc north of the Ahel cluster, and (3) part of the coastal Fars arc between the Ahel and Fin-Tiab clusters (Figures 1b, 2b, and 3)). Rarely, there are events common to a pair of overlapping clusters. In these instances, we find that the 90% confidence bounds on the common event epicenter overlap, but we present only the location with the better azimuthal coverage and lower uncertainty.

We gathered data from local catalogs including the Iranian National Seismograph Network, the Iranian Building and Housing Research Network (BHRC), the Iranian Seismological Center, as well as temporary deployments in Iran and neighboring countries. The station coordinates are corrected according to the issues documented by Syracuse et al. (2017). To improve connectivity at regional and teleseismic distances, we also included data from the ISC Bulletin (including both reviewed and unreviewed events) and from the USGS NEIC. The distance limit over which the hypocentroid is calculated depends upon data availability and azimuthal coverage, and therefore varies between clusters (Figures S2–S17). In most cases it approximates or exceeds 1.0°, but in cases like the Dehloran cluster it was selected as 0.6° (Figure S5), allowing us to

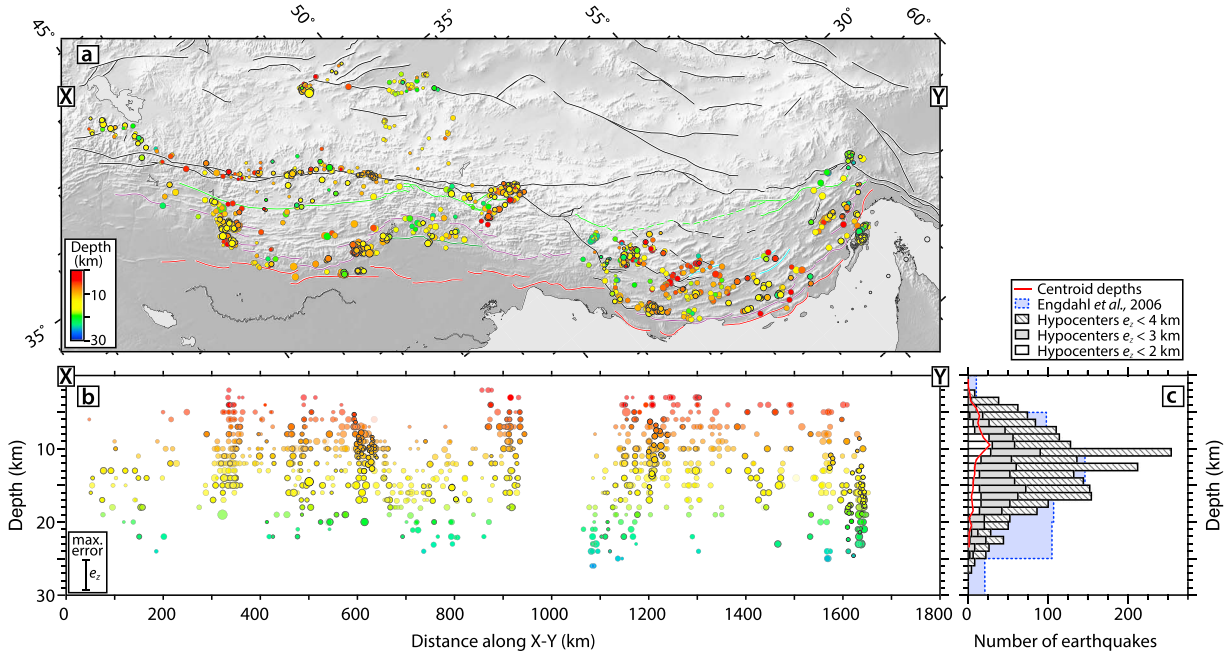

Figure 5. (a) Calibrated epicentral locations plotted in an oblique Mercator projection with equator azimuth N130°E. Events with robust focal depths are colored accordingly. Major surface-breaking faults are in black and Berberian's (1995) "master blind thrusts" are in color (for names, see Figure 1b). (b) The same earthquakes projected onto the line X-Y and plotted in depth section; solid circles show free-depth solutions and focal depths estimated with near-distance arrival times; faint circles show focal depths determined with local-distance arrival times and depth phases. (c) Earthquake depth distributions. Focal depths determined with local-distance arrival times and depth phases are hashed, those from near-distance arrival times are in gray, and free-depth solutions are in white. The previous best focal depth estimates of Engdahl et al. (2006) are in blue, binned at 5 km rather than 1 km intervals and excluding deeper Oman Line events which in their catalog reach depths of ~45 km. The red line shows the *centroid* depth distribution from published teleseismic body waveform studies, updated from Nissen et al. (2011).

avoid difficulties introduced by incorporating *Pn* and *Sn* readings (Figure S5c). In cases where calibration is made difficult by limited availability of regional data, large open azimuths (>220°), or strong lateral velocity heterogeneity, events can be relocated using both the direct and indirect calibration techniques. We chose to use indirect calibration for the recent Ezgeleh-Sarpolzahab sequence (Polzohab2 in Table S1) and for the Shushtar and Fin-Tiab clusters (Figures S17 and S8), though in none of these cases do we rely upon InSAR-derived finite fault models (cf. Copley et al., 2015).

For each cluster we developed a custom crustal model by fitting *P* and *S* waves to the available arrival data in the source region (Figure 4). Although the effect of unknown velocity model is minimized for the calculation of cluster vectors, the subset of theoretical traveltimes used to estimate the hypocentroid can potentially bias our locations and hence requires further adjustment. This is done by fitting close-in, shorter (and preferably direct) ray paths from multiple events with fixed relative locations. As long as the azimuthal coverage is good at this distance range, the hypocentroid will remain stable even with variations in the local crustal model, and a stable velocity structure can be obtained. Once direct phases (*Pg*, *Sg*) are adjusted, crustal thickness and then lower crustal velocities can be determined by fitting *Pn* and *Sn* arrival times. The *ak*135 1-D average global model (Kennett et al., 1995) is used for regional and teleseismic distances. The fit to the model at these distances (Figures S2e, S2f–S17e, and S17f) does not affect calibration of the cluster since these data are only used for relative location calculations. Our 1-D local models are composed of two to three layered crust with average *P* and *S* wave velocities of 5.5 and 3.1 km/s for the upper crust and 6.2 and 3.6 km/s for the lower crust (Figure 4), in close agreement with values obtained from local microseismic studies (Hatzfeld et al., 2003; Nissen et al., 2010, 2011; Tatar et al., 2004; Yamini-Fard et al., 2012). Moho depths range from 44 to 55 km, with slightly thicker average values in the northwestern Zagros (~50 km) than in the southeastern Zagros (~46 km). Although our estimates of crustal thickness are averaged over ~100-km length scales, they broadly agree with the local crustal thickness estimates of 42–58 km determined from receiver function studies (Afsari et al., 2011; Hatzfeld et al., 2003; Paul et al., 2010; Tatar & Nasrabadi, 2013).

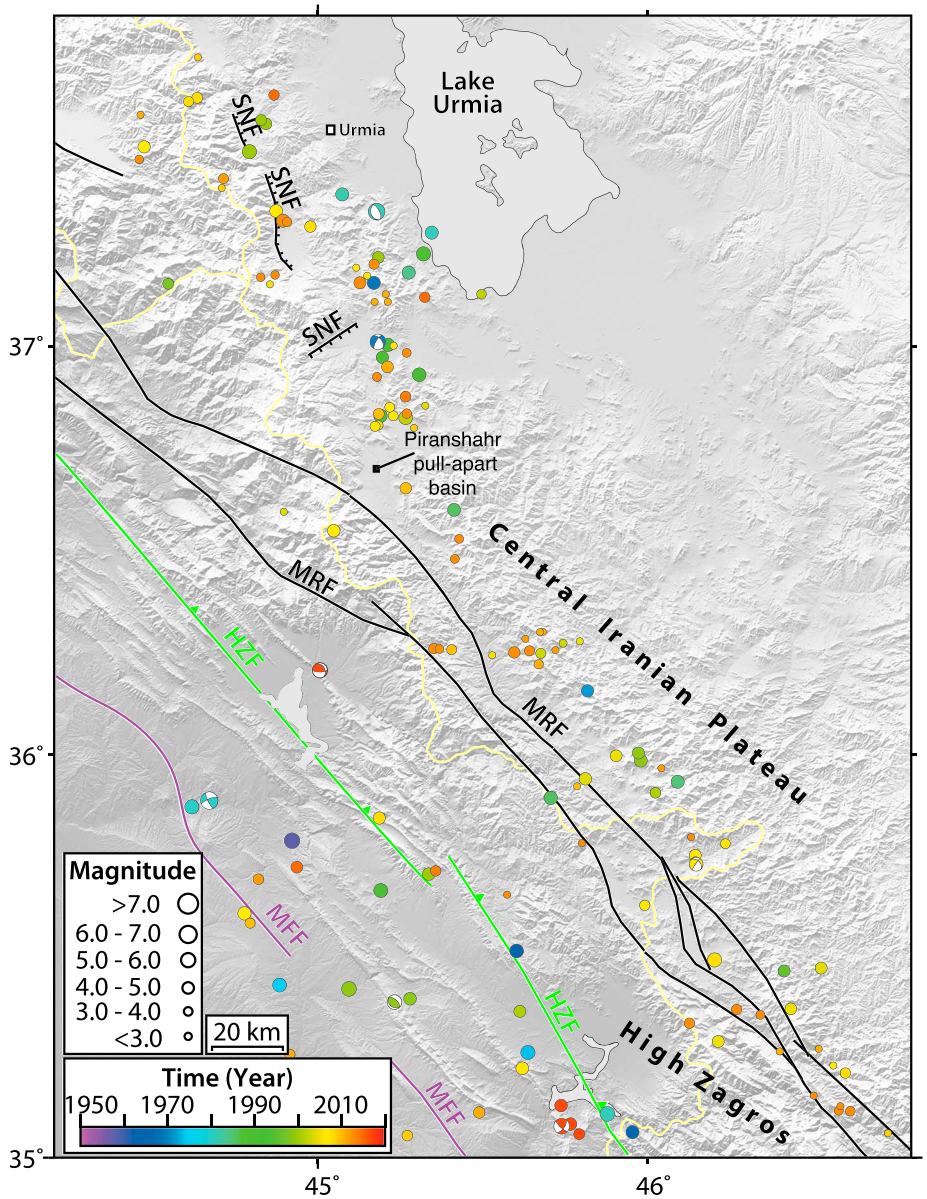

Figure 6. Close-up map of calibrated earthquake epicenters in the northern Zagros, colored by time and scaled by magnitude, showing the deviation of seismicity from the Main Recent Fault (MRF). Where they are available (from the references listed in Table S2), teleseismic focal mechanisms are plotted at their relocated epicenters using the same scaling and coloring. Major surface-breaking faults are in black and Berberian's (1995) "master blind thrusts" are in color. HZF = High Zagros Fault; MFF = Mountain Front Fault; SNF = Serow Normal Faults (Copley & Jackson, 2006).

4. Results

We used 17 clusters in the Zagros and adjacent regions of the Iranian plateau to relocate 2,424 events from 1951 to 2018, including 267 events of M_w 4.8–7.3 that have published or catalog focal mechanisms (Figures 1b, 1c, and Figures S2–S17; Table S1). Details of individual clusters are provided in the supporting information. The 135 events before 1980 are now calibrated, including the destructive 1962 M_w 7.0 Buyin-Zara, 1972 M_w 6.7 Ghir, and 1977 M_w 6.7 Khurgu earthquakes. All calibrated events have location errors less than 5 km, and ~80% have uncertainties less than 3 km. Shift vectors linking initial catalog locations (mostly from the ISC) with final calibrated locations average ~11 km and reach a maximum of ~111 km (Figure 1c). The dominant azimuthal shift is to the N and NE along most of the Zagros, partly reflecting the poor station distribution to the S and SW. However, the dominant azimuthal shift is to the E in the

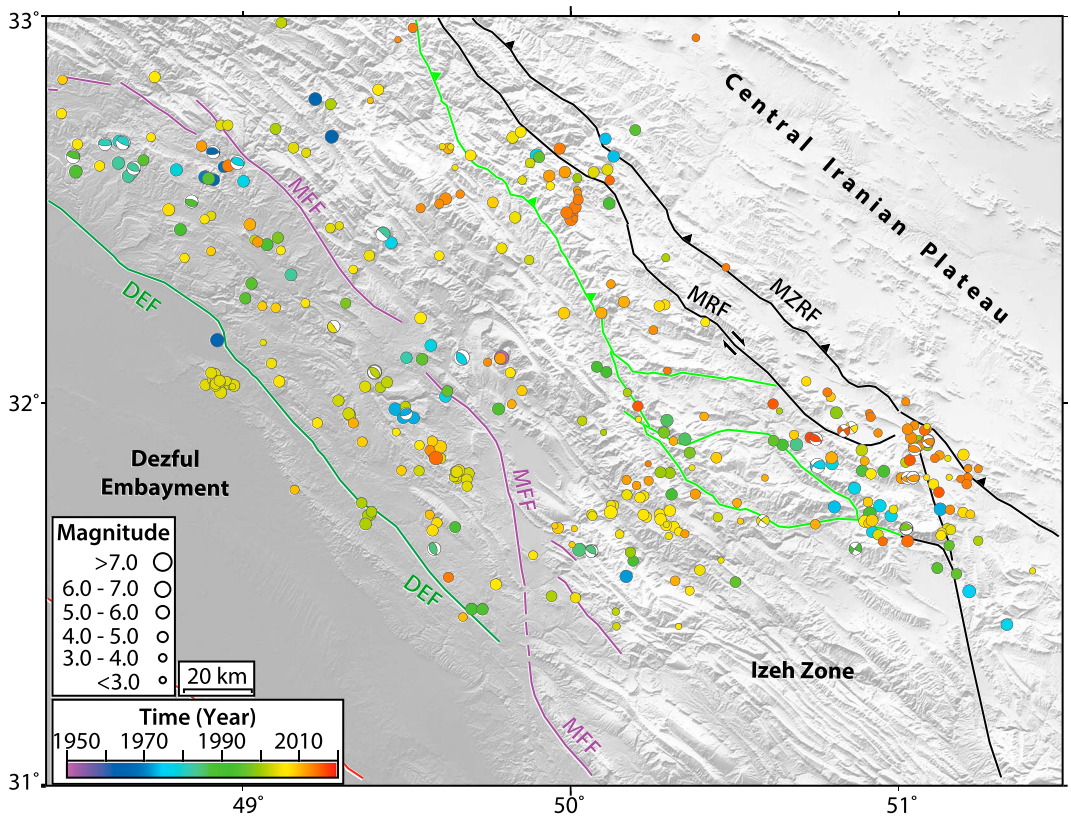

Figure 7. Close-up map of calibrated earthquake epicenters in the Dezful embayment and Izeh zone, colored by time and scaled by magnitude, showing the intense and scattered seismicity between the Dezful Embayment Fault (DEF) and High Zagros Fault (HFF). Where they are available (from the references listed in Table S2), teleseismic focal mechanisms are plotted at their relocated epicenters using the same scaling and coloring. Major surface-breaking faults are in black and Berberian's (1995) "master blind thrusts" are in color. MFF = Mountain Front Fault; MRF = Main Recent Fault; MZRF = Main Zagros Reverse Fault.

Shushtar and Farsan clusters, and to the NW in the easternmost Fin-Tiab cluster, indicating important local and regional velocity perturbations.

Using the analysis described in section 3 we calibrated depths of ~1,100 events (Figure 5 and Table S1). This revealed a ~24-km-thick seismogenic layer with a peak in the focal depth distribution at 10–13 km (Figure 5c). Among these, 673 events have focal depths constrained by local-distance arrival times, with ~4 km errors, and 420 events have focal depths set by free-depth inversions or by exploiting near-distance arrival times, with <3 km errors. For 14 events in this study, we used depth phases to set the focal depths. These are preferred for events with no information on focal depth from near- or local-distance data, but with enough depth phase picks (at least 4–5 picks) to set focal depths. We used bulletin picks and did not employ any additional weighing for depth phases.

4.1. Northwestern Zagros

We observe abundant seismicity along much of the mapped trace of the central part of the Main Recent Fault, between ~33.5°N and ~35.5°N (Figure 2). However, outside of these latitudes we observe significant deviations of seismicity away from this trace (Figures 2 and 6). In our Oshnaviyeh cluster in the northern Zagros, seismicity concentrates NE of the Main Recent Fault, onto a suite of short, oblique (dextral-normal) faults mapped on the basis of range front geomorphology by Copley and Jackson (2006). This deviation of seismicity northward from the Main Recent Fault starts at the Piranshahr pull-apart basin and continues toward the Serow normal faults west of the Lake Urumieh (Figure 6). Our calibrated epicenters north of the Piranshahr pull-apart, including the 1970 M_w 5.5 earthquake, are consistent with the NE or SE dip directions of the faults that Copley and Jackson (2006) mapped (see their Figure 7).

We were only able to generate three calibrated clusters in the central Iranian plateau, at Avaj, Qom, and Aligudarz (Figure 2). Newly calibrated earthquakes include the 1967 M_w 7.0 Buyin-Zara, 2002 M_w 6.4 Changureh, and 2007 M_w 5.7 Qom earthquakes. Most of the seismicity appears to align with known active faults (Figure 2), and we do not spend further time discussing this area.

In the south, we observe a concentration of seismicity around the intersections of the High Zagros, Main Recent, and Main Zagros Reverse Fault traces, including strike-slip and thrust earthquakes with a variety of trends (Figure 2). Southwest of the Main Recent Fault, the Sahneh and Dorud clusters highlight scattered seismicity in the northwestern High Zagros, with only a few events consistent with the mapped trace of the High Zagros Fault (Figure 2). In contrast, seismicity in the Lurestan arc is focused strongly along the frontal escarpments and the mapped locations of the Zagros Foredeep and Mountain Front Faults. This includes the recent M_w 7.3 Ezgeleh-Sarpolzahab (2017) sequence, which ruptured an E dipping (~15°) dextral-thrust basement fault in the northern Lurestan arc that is approximately colocated with, albeit highly oblique to Berberian's (1995) Mountain Front Fault (e.g., Barnhart et al., 2018; Chen et al., 2018; Nissen et al., 2019). Several of the other mainshock-aftershock sequences in the Lurestan arc, such as at Moosiyan (2008, 2012), Qasr-e Shirin (2013), Murmuri (2014), and Mandali (2018), also appear to have ruptured the Zagros Foredeep or Mountain Front Faults (Copley et al., 2015; Nippress et al., 2017; Nissen et al., 2019).

The 2008 Moosiyan and 2014 Murmuri sequences were previously relocated in *mloc* using an indirect calibration, forced by the large (~180°) azimuthal gap in close-in arrival data at southern azimuths (Copley et al., 2015). In their study, the entire cluster was calibrated using InSAR-derived model fault planes for the 27 August 2008 and 15 October 2014 earthquakes, which resulted in epicentral errors exceeding ~10 km (set by the large fault plane dimensions). We updated this cluster with additional 15 events recorded by a temporary array in 2014, which greatly reduced the azimuthal gap in close-in arrival data, and permitted a direct calibration of the entire cluster with much lower hypocenter errors (<4 km). This significant improvement over indirect calibration caused the mainshock epicenters to move ~3 km to the NW relative to the locations in Copley et al. (2015). Nevertheless, our new calibrated locations confirm Copley et al.'s (2015) interpretation that the 18 August 2014 Murmuri mainshock and its largest aftershock ruptured N dipping planes. The even distribution of aftershock locations along-strike of this mainshock fault plane supports a bilateral rupture.

We observe intense, scattered seismicity in the northern Dezful embayment and adjacent parts of the High Zagros (Figure 2). This region experienced several older (1980–2005) M_w 5.0–5.6 earthquakes, most of which are included in the Shushtar cluster, one of three that we calibrated indirectly using events from a local temporary network (Table S1). Many of the $M_w > 5$ epicenters are consistent with rupture of the Dezful Embayment or Mountain Front Faults, but several moderate earthquakes occur off these faults, especially within the Izeh zone, a region of tight folding and structural complexity between the Mountain Front and High Zagros Faults (Figure 7). The highly diffuse pattern of seismicity, and the large concentration of M_w 5.0–5.6 events, implies that seismogenic structures in this region are mostly broken up into short fault segments.

4.2. Southeastern Zagros

The Fars arc generally displays diffuse seismicity, with a larger proportion of earthquakes situated away from the frontal Zagros Foredeep and Mountain Front Faults, exposing several previously unmapped faults in the range interior (Figure 3). In the northern Karbaas cluster, we confirm that the N-S trending Kazerun, Kareh Bas and Sabz Pushan strike-slip faults are all seismically active but also reveal new trends in seismicity, in particularbetween the Kazerun and Kareh Bas faults (Figure 8). Some of these trends align ~E–W and may involve left-lateral faulting that is conjugate to the main N–S faults, in a pattern of "bookshelf faulting" reminiscent of other parts of Iran (e.g., Penney et al., 2015; Walker & Jackson, 2004). The Sarvestan fault is not included in any of our clusters due to a lack of nearby data.

The Kaki cluster to the south is based around the 2013 M_w 6.2 Kaki earthquake, which from InSAR modeling ruptured two SW-dipping reverse faults near the southern termination of the Kazerun fault (Elliott et al., 2015; Figure 3). The clear trend in epicenters in this region is consistent with rupture on, or just north of, the Mountain Front Fault (Figure 3). Likewise, seismicity clusters along Berberian's (1995) E–W trending Surmeh fault, which we can confirm likely hosted the M_w 6.7 Ghir (1972) earthquake and its aftershock sequence. However, we also observe abundant moderate-sized events in between the Surmeh and Mountain Front Faults, including several clusters or trends that appear to illuminate important, unnamed faults. For

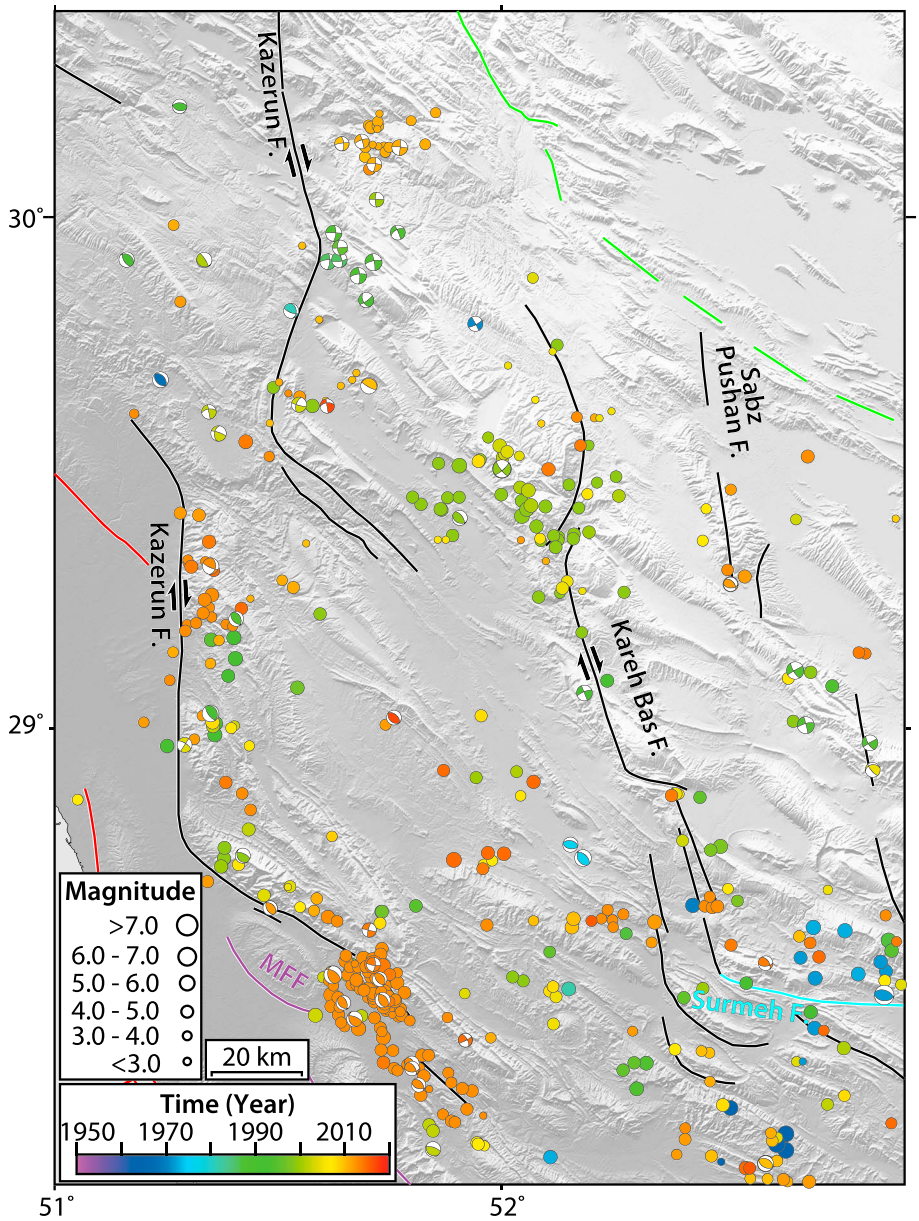

Figure 8. Close-up map of calibrated earthquake epicenters in the northern Fars Arc, colored by time and scaled by magnitude, showing the area with possible conjugate left-lateral faulting lie east of the northern strand of the Kazerun fault. Where they are available (from the references listed in Table S2), teleseismic focal mechanisms are plotted at their relocated epicenters using the same scaling and coloring. Major surface-breaking faults are in black and Berberian's (1995) "master blind thrusts" are in color. MFF = Mountain Front Fault.

example, seismicity south of the Surmeh fault aligns with the Kuh-e Halikan anticline, hinting that this fold may also be cored by a large reverse fault.

In the Ahel cluster, our earthquake locations are localized along, and also in between Berberian's (1995) E-W trending Mountain Front, Zagros Foredeep, Beriz, and Lar Faults (Figure 3). This cluster includes four moderate magnitude (M_w 5.1–5.8), previously published InSAR events: 5 May 1997, 18 September 1997, 30 April 1999 (Lohman & Simons, 2005), and 20 July 2010 (Barnhart et al., 2013). Our calibrated hypocenters for three of these events align well with these published fault models; but the fourth—the 18 September 1997 earthquake—lies ~8 km north of the InSAR source model. This discrepancy might reflect a relatively poor InSAR signal and/or the ~3-year time span of the interferogram which may have captured other sources of deformation.

Among our calibrated clusters in the Fars arc, the High Zagros Fault is only well-covered by the easternmost Fin-Tiab cluster, where it is clearly seismically active (Figure 3). This is the second of our indirect calibration clusters, in which we utilized well-relocated events in the eastern Tiab region to solve the azimuthal gap problem in the western Fin region. Seismicity in the southeastern Fars arc includes clear streaks along segments of the Mountain Front Fault, which we can confirm hosted the M_w 6.7 Khurgu (1977) earthquake and several of its largest aftershocks. However, the 2005–2008 Qeshm and 2006 Fin sequences both lie off Berberian's (1995) mapped faults; these sequences are described in more detail elsewhere (Nissen et al., 2010; Roustaei et al., 2010).

5. Discussion

5.1. Master Blind Thrust Faults

Our calibrated relocations reveal distinct patterns of seismicity in the Lurestan arc in the northwestern Zagros, the Dezful embayment in the central Zagros, and the Fars arc in the southeastern Zagros. In the Lurestan arc (Figure 2), most seismicity collapses onto the frontal escarpment, primarily along the Zagros Foredeep and Mountain Front Faults. The low level of seismicity within the interior Lurestan arc and adjacent High Zagros supports Berberian's (1995) interpretation that seismic hazard is heavily concentrated along the master blind thrusts. However, more gently dipping faulting responsible for the recent M_w 7.3 Ezgeleh-Sarpolzohab earthquake may underlie interior parts of the Lurestan arc, as discussed by Nissen et al. (2019). Seismicity is much more diffuse in the Dezful embayment where we observe activity concentrated in the interior embayment both on and in between the master thrust faults (Figure 7).

This scattered seismicity is more evident still throughout the Fars arc (Figure 3). Among (Berberian, 1995)'s master thrust faults, the Mountain Front Fault appears active throughout the Fars arc, rupturing in the 1977 M_w 6.7 Khurgu earthquake among other events, and the interior Surmeh and Beriz faults also host significant earthquakes including the 1972 M_w 6.7 Ghir earthquake. However, only near Ahel do we observe clear seismicity on the Zagros Foredeep Ffault, and we observe numerous seismicity trends in between these mapped faults. Hence, seismicity in the Fars arc requires that there are numerous smaller buried faults within the folded cover, and which might plausibly control fold development (e.g., Alavi, 2007; McQuarrie, 2004). This hints at a more direct, causative relationship between reverse faulting and surface anticline growth in the Fars arc than in the northwestern Zagros.

The contrasting seismicity patterns of the Lurestan and Fars arcs may be related to differences in the large-scale topography and crustal structure in the two regions (Motaghi, Shabanian & Kalvandi 2017; Motaghi, Shabanian, Tatar, et al., 2017). The topographic taper of the Lurestan arc is significantly steeper than that of the Fars arc, as indicated by the closer spacing of smoothed topographic contours in Figure 1b. Gravitational driving forces arising from gradients in topography are thus concentrated around the edge of the Lurestan arc, where they are known to have a role in generating seismicity (Copley et al., 2015), but spread more evenly across the Fars arc. Differences in the distribution of Hormuz salt deposits, which are thickest in the Fars arc, and other lateral changes in the sedimentary sequence may also play a role in focusing or defocusing seismicity, though the causative mechanism is not clear.

5.2. Depth

Our minimally biased hypocenter relocation procedure has significantly improved our ability to resolve focal depths in the Zagros. The ~1,100 events with robust focal depths indicate a seismogenic depth range of ~4–25 km (Figures 5a and 5b), and a relatively balanced distribution between the basement and the sedimentary cover. The concentration of deeper seismicity at the southeast end of the profile (x axis distances >1,600 km) mimics a known trend in centroid depths known as the Oman Line (e.g., Talebian & Jackson, 2004). Compared to the previous best available catalog of focal depths in Iran (Engdahl et al., 2006), our new focal depths are in much better agreement with independent centroid depth estimates of ~100 larger earthquakes constrained by teleseismic body waveform modeling (Figure 5c). In contrast, Engdahl et al. (2006) placed a much larger proportion of Zagros earthquakes in the 20- to 30-km depth range and a few events deeper than 30 km, increasing to up to ~45 km along the Oman Line.

The peak in our focal depth distribution, at ~10–13 km, is slightly deeper than the peak in centroid depths, at ~9 km, but we consider this unsurprising since most larger events are expected to nucleate near the base of the fault (for a deeper focal depth) and then rupture upward (for a shallower centroid depth). This is illustrated in Figure 9, which shows that for 32 larger ($M_w > 5$) earthquakes for which robust estimates of

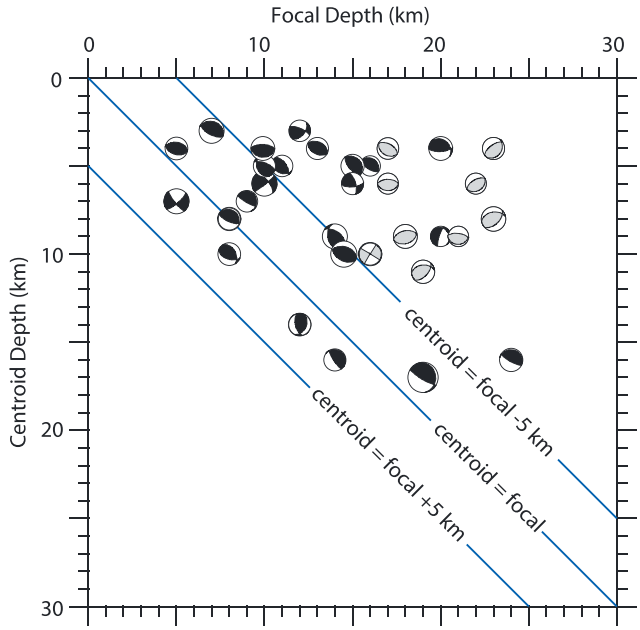

Figure 9. Focal mechanisms of several larger earthquakes for which robust estimates of both centroid (from published waveform modeling studies in Table S2) and focal depth (from this study) are available. Gray focal mechanisms are from the Qeshm cluster.

both centroid and focal depth are available, there exists a clear bias toward deeper focal depths. Individual events in the Qeshm (shown in gray in Figure 9) cluster have significantly deeper focal depths than their centroid depths (6–19 km), suggesting a complex process of rupture nucleation and propagation that lies beyond the scope of this study.

6. Conclusions

We have determined ~2,500 calibrated earthquake epicenters with ~1,100 robust focal depths spanning most of the Zagros orogen. In the northwestern High Zagros, we reveal epicentral trends that deviate from the mapped trace of the Main Recent Fault, confirming the dextral-normal faulting previously recognized by Copley and Jackson (2006). In the Simply Folded Belt, we observe a clear distinction between the Lurestan arc, where seismicity focuses along major mapped frontal faults, and the Fars arc, where there is a larger proportion of out-of-sequence thrusting including numerous unmapped faults. This hints at a difference in the relationship between folding and faulting in the two regions. We also observe new seismicity trends in the central Zagros, which may indicate previously unrecognized conjugate E–W left-lateral faults between the N–S right-lateral Kazerun and Kareh Bas faults. Overall, our focal depth distribution of 4–25 km implies earthquakes nucleate within both the basement and the sedimentary cover, in roughly similar proportions, and is broadly consistent with the centroid depth distribution of ~100 larger earthquakes previously constrained by teleseismic body waveform modeling. In contrast with previous hypocenter catalogs in the Zagros, we see no evidence for foci deeper than ~30 km.

Acknowledgments
This work was supported by the National Science Foundation through Grant EAR 1524815. E. N. acknowledges additional support from the Natural Sciences and Engineering Research Council of Canada (NSERC) through Discovery Grant 2017-04029, the Canada Foundation for Innovation (CFI), the British Columbia Knowledge Development Fund (BCKDF), and the Canada Research Chair program. We are grateful to two anonymous reviewers for their thorough and thoughtful reviews of the manuscript. Local network data used in this work belong to the Institute for Advanced Studies in Basic Sciences (IASBS) and the Geological Survey of Iran. Phase arrival time data, most of which are freely available, were gathered from the Iranian National Seismograph Network (INSN, http://www.iiees.ac.ir/en/), the Iranian Building and Housing Research Network (BHRC, https://ismn.bhrc.ac.ir/en/), the Iranian Seismological Center (IRSC, http://irsc.ut.ac.ir/), the United States Geological Survey (USGS, https://earthquake.usgs.gov/earthquakes/), and the International Seismological Centre (ISC, http://www.isc.ac.uk/iscbulletin/search/bulletin/). Most of the local-distance phase arrivals were picked by Abdolreza Ghods and his research group at the Department of Earth Sciences, IASBS. We also used phase arrival time data from temporary networks deployed by Farzam Yamini-Fard and Mohammad Tatar (IIEES). All of the calibrated locations in this study are available in the Global Catalog of Calibrated Earthquake Locations (GCCEL) website (https://www.sciencebase.gov/catalog/item/59fb91fde4b0531197b16ac7). Most of the figures were plotted using Generic Mapping Tools (Wessel et al., 2013).

References

Abdollahie-Fard, I., Braathen, A., Mokhtari, M., & Alavi, S. A. (2006). Interaction of the Zagros fold–thrust belt and the Arabian-type, deep-seated folds in the Abadan plain and the Dezful embayment, SW Iran. *Petroleum Geoscience*, *12*(4), 347–362.

Afsari, N., Sodoudi, F., Farahmand, F. T., & Ghassemi, M. R. (2011). Crustal structure of northwest Zagros (Kermanshah) and Central Iran (Yazd and Isfahan) using teleseismic PS converted phases. *Journal of Seismology*, *15*(2), 341–353.

Ahmadhadi, F., Lacombe, O., & Daniel, J. M. (2007). Early reactivation of basement faults in Central Zagros (SW Iran): evidence from pre-folding fracture populations in Asmari Formation and lower Tertiary paleogeography, *Thrust Belts and Foreland Basins* pp. 205–228). Berlin Heidelberg: Springer.

Alavi, M. (2007). Structures of the Zagros fold-thrust belt in Iran. *American Journal of Science*, *307*, 1064–1095.

Allen, M. B., Saville, C., Blanc, E. J. P., Talebian, M., & Nissen, E. (2013). Orogenic plateau growth: Expansion of the Turkish-Iranian plateau across the Zagros fold-and-thrust belt. *Tectonics*, *32*, 171–190. https://doi.org/10.1002/tect.20025

Ambraseys, N. N., & Melville, C. P. (1982). *A history of Persian earthquakes*. Cambridge: Cambridge University Press.

Ambraseys, N. N., & Moinfar, A. A. (1973). The seismicity of Iran. The Silakhor, Lurestan, earthquake of 23rd January, 1909. *Annali di Geofisica*, *26*(4), 659–678.

Authemayou, C., Bellier, O., Chardon, D., Benedetti, L., Malekzade, Z., Claude, C., & Abbassi, M. R. (2009). Quaternary slip-rates of the Kazerun and the main recent faults: Active strike-slip partitioning in the Zagros fold-and-thrust belt. *Geophysical Journal International*, *178*, 524–540.

Authemayou, C., Chardon, D., Bellier, O., Malekzadeh, Z., Shabanian, E., & Abbassi, M. R. (2006). Late Cenozoic partitioning of oblique plate convergence in the Zagros fold-and-thrust belt (Iran). *Tectonics*, *25*, TC3002. https://doi.org/10.1029/2005TC001860

Aziz Zanjani, A., Ghods, A., Sobouti, F., Bergman, E., Mortezanejad, G., Priestley, K., et al. (2013). Seismicity in the western coast of the South Caspian basin and the Talesh Mountains. *Geophysical Journal International*, *195*, 799–814.

Baker, C. (1993). *The active seismicity and tectonics of Iran*. Cambridge, UK: University of Cambridge.

Baker, C., Jackson, J., & Priestley, K. (1993). Earthquakes on the Kazerun line in the Zagros mountains of Iran: Strike-slip faulting within a fold-and-thrust belt. *Geophysical Journal International*, *115*, 41–61.

Ballato, P., Nowaczyk, N. R., Landgraf, A., Strecker, M. R., Friedrich, A., & Tabatabaei, S. H. (2008). Tectonic control on sedimentary facies pattern and sediment accumulation rates in the Miocene foreland basin of the southern Alborz mountains, northern Iran. *Tectonics*, *27*, TC6001. https://doi.org/10.1029/2008TC002278

Barnhart, W. D., Brengman, C. M. J., Li, S., & Peterson, K. E. (2018). Ramp-flat basement structures of the Zagros mountains inferred from co-seismic slip and afterslip of the 2017 M_w7.3 Darbandikhan, Iran/Iraq earthquake. *Earth and Planetary Science Letters*, *496*, 96–107. https://doi.org/10.1016/j.epsl.2018.05.036

Barnhart, W. D., & Lohman, R. B. (2013). Phantom earthquakes and triggered aseismic creep: Vertical partitioning of strain during earthquake sequences in Iran. *Geophysical Research Letters*, *40*, 819–823. https://doi.org/10.1002/grl.50201

Barnhart, W. D., Lohman, R. B., & Mellors, R. J. (2013). Active accommodation of plate convergence in Southern Iran: Earthquake locations, triggered aseismic slip, and regional strain rates. *Journal of Geophysical Research: Solid Earth*, *118*, 5699–5711. https://doi.org/10.1002/jgrb.50380

Berberian, M. (1979). Earthquake faulting and bedding thrust associated with the Tabas-e-Golshan (Iran) earthquake of September 16, 1978. *Bulletin of the Seismological Society of America*, *69*, 1861–1887.

Berberian, M. (1981). Active faulting and tectonics of Iran, *Zagros Hindu Kush Himalaya Geodynamic Evolution* (pp. 33–69). Washington, DC: American Geophysical Union.

Berberian, M. (1995). Master blind thrust faults hidden under the Zagrosfolds: Active basement tectonics and surface morphotectonics. *Tectonophys*, *241*, 193–224.

Berberian, M. (2014). *Earthquakes and coseismic surface faulting on the Iranian Plateau* (Vol. 17). Amsterdam, Netherlands: Elsevier.

Berberian, M., & King, G. C. P. (1981). Towards a paleogeography and tectonic evolution of Iran. *Canadian Journal of Earth Sciences*, *18*(2), 210–265. https://doi.org/10.1139/e81-019

Berberian, M., & Tchalenko, J. S. (1976). Earthquakes of Bandar Abbas–Hajiabad Region (Zagros, Iran). *Geological Survey of Iran*, *39*, 371–396.

Berberian, M., & Yeats, R. S. (2001). Contribution of archaeological data to studies of earthquake history in the Iranian Plateau. *Journal of Structural Geology*, *23*, 563–584. https://doi.org/10.1016/S0191-8141(00)00115-2

Bergman, E. A., & Solomon, S. C. (1990). Earthquake swarms on the Mid-Atlantic Ridge—Products of magmatism or extensional tectonics? *Journal of Geophysical Research*, *95*, 4943–4965.

Blanc, E. J. P., Allen, M. B., Inger, S., & Hassani, H. (2003). Structural styles in the Zagros simple folded zone, Iran. *Journal of the Geological Society London*, *160*, 401–412.

Carruba, S., Perotti, C. R., Buonaguro, R., Calabrò, R., Carpi, R., & Naini, M. (2006). Structural pattern of the Zagros fold-and-thrust belt in the Dezful embayment (SW Iran). *Geological Society of America Special Papers*, *414*, 11–32.

Casciello, E., Vergés, J., Saura, E., Casini, G., Fernández, N., Blanc, E., & Hunt, D. W. (2009). Fold patterns and multilayer rheology of the Lurestan Province, Zagros Simply Folded Belt (Iran). *Journal of the Geological Society London*, *166*, 947–959.

Chen, K., Xu, W., Mai, P. M., Gao, H., Zhang, L., & Ding, X. (2018). The 2017 M_w 7.3 Sarpol Zahāb Earthquake, Iran: A compact blind shallow-dipping thrust event in the mountain front fault basement. *Tectonophysics*, *747*, 108–114. https://doi.org/10.1016/j.tecto.2018.09.015

Colman-Sadd, S. P. (1978). Fold development in Zagros Simply Folded Belt, Southwest Iran. *American Association of Petroleum Geologists Bulletin*, *62*, 984–1003.

Copley, A., & Jackson, J. (2006). Active tectonics of the Turkish-Iranian Plateau. *Tectonophys*, *25*, TC6006. https://doi.org/10.1029/2005TC001906

Copley, A., Karasozen, E., Oveisi, B., Elliott, J. R., Samsonov, S., & Nissen, E. (2015). Seismogenic faulting of the sedimentary sequence and laterally variable material properties in the Zagros Mountains (Iran) revealed by the August 2014 Murmuri (E. Dehloran) earthquake sequence. *Geophysical Journal International*, *203*, 1436–1459. https://doi.org/10.1093/gji/ggv365

Croux, C., & Rousseeuw, P. J. (1992). Time-efficient algorithms for two highly robust estimators of scale. In Y. Dodge & J. Whittaker (Eds.), *Computational Statistics* (pp. 411–428). Heidelberg: Physica-Verlag.

Derikvand, B., Alavi, S. A., Fard, I. A., & Hajialibeigi, H. (2018). Folding style of the Dezful embayment of Zagros belt: Signatures of detachment horizons, deep-rooted faulting and syn-deformation deposition. *Marine and Petroleum Geology*, *91*, 501–518.

Devlin, S., Isacks, B. L., Pritchard, M. E., Barnhart, W. D., & Lohman, R. B. (2012). Depths and focal mechanisms of crustal earthquakes in the central Andes determined from teleseismic waveform analysis and InSAR. *Tectonics*, *31*, TC2002. https://doi.org/10.1029/2011TC002914

Donner, S., Krüger, F., Rößler, D., & Ghods, A. (2014). Combined inversion of broadband and short-period waveform data for regional moment tensors: A case study in the Alborz Mountains, Iran. *Bulletin of the Seismological Society of America*, *104*(3), 1358–1373.

Donner, S., Rößler, D., Krüger, F., Ghods, A., & Strecker, M. R. (2013). Segmented seismicity of the M_w 6.2 Baladeh earthquake sequence (Alborz Mountains, Iran) revealed from regional moment tensors. *Journal of Seismology*, *17*, 925–959.

Dziewonski, A. M., Chou, T. A., & Woodhouse, J. H. (1981). Determination of earthquake source parameters from waveform data for studies of global and regional seismicity. *Journal of Geophysical Research*, *86*, 2825–2852.

Ekström, G. (1989). A very broad band inversion method for the recovery of earthquake source parameters. *166*, 73–100. https://doi.org/10.1016/0040-1951(89)90206-0

Ekström, G., Nettles, M., & Dziewoński, A. M. (2012). The global CMT project 2004–2010: Centroid-moment tensors for 13,017 earthquakes. *Physics of the Earth and Planetary Interiors*, *200*, 1–9. https://doi.org/10.1016/j.pepi.2012.04.002

Elliott, J. R., Bergman, E. A., Copley, A. C., Ghods, A. R., Nissen, E. K., Oveisi, B., & Yamini-Fard, F. (2015). The 2013 M_w 6.2 Khaki-Shonbe (Iran) earthquake: Insights into seismic and aseismic shortening of the Zagros sedimentary cover. *Earth and Space Science*, *2*, 435–471. https://doi.org/10.1002/2015EA000098

Engdahl, R. E., Jackson, J. A., Myers, S. C., Bergman, E. A., & Priestley, K. (2006). Relocation and assessment of seismicity in the Iran region. *Geophysical Journal International*, *167*, 761–778.

Engdahl, E. R., van der Hilst, R. D., & Buland, R. (1998). Global teleseismic earthquake relocation from improved travel times and procedures for depth determination. *Bulletin of the Seismological Society of America*, *88*, 722–743.

Fakhari, M. D., Axen, G. J., Horton, B. K., Hassanzadeh, J., & Amini, A. (2008). Revised age of proximal deposits in the Zagros foreland basin and implications for Cenozoic evolution of the High Zagros. *Tectonophys*, *451*, 170–185.

Falcon, N. L. (1969). Problems of the relationship between surface structure and deep displacements illustrated by the Zagros Range. *Geological Society, London, Special Publications*, *3*(1), 9–21.

Falcon, N. L. (1974). Southern Iran: Zagros Mountains. *Geological Society, London, Special Publications*, *4*(1), 199–211.

Farzipour-Saein, A., Yassaghi, A., Sherkati, S., & Koyi, H. (2009). Mechanical stratigraphy and folding style of the Lurestan region in the Zagros fold–thrust belt, Iran. *Journal of the Geological Society*, *6*, 1101–1115.

Ghods, A., Rezapour, M., Bergman, E., Mortezanejad, G., & Talebian, M. (2012). Relocation of the 2006 M_w 6.1 Silakhour, Iran, earthquake sequence: Details of Fault Segmentation on the Main Recent Fault. *Bulletin of the Seismological Society of America*, *102*, 398–416.

Guest, B., Horton, B. K., Axen, G. J., Hassanzadeh, J., & McIntosh, W. C. (2007). Middle to late Cenozoic basin evolution in the western Alborz Mountains: Implications for the onset of collisional deformation in northern Iran. *Tectonics*, *26*, TC6011. https://doi.org/10.1029/2006TC002091

Hatzfeld, D., Tatar, M., Priestley, K., & Ghafory-Ashtiany, M. (2003). Seismological constraints on the crustal structure beneath the Zagros Mountain belt (Iran). *Geophysical Journal International*, *155*, 403–410.

Havskov, J., & Ottemoller, L. (2010). Location, *Routine data processing in earthquake seismology* (pp. 101–149). Dordrecht: Springer. https://doi.org/10.1007/978-90-481-8697-6

Hessami, K., Koyi, H. A., & Talbot, C. J. (2001). The significance of strike-slip faulting in the basement of the Zagros fold and thrust belt. *Journal of Petroleum Geology*, *24*, 5–28.

Hessami, K., Koyi, H. A., Talbot, C. J., Tabasi, H., & Shabanian, E. (2001). Progressive unconformities within an evolving foreland fold thrust belt, Zagros Mountains. *Journal of the Geological Society London*, *158*, 969–981.

Homke, S., Verges, J., Serra-Kiel, J., Bernaola, G., Sharp, I., Garces, M., & Goodarzi, M. H. (2009). Late Cretaceous-Paleocene formation of the proto-Zagros foreland basin, Lurestan Province, SW Iran. *Geological Society of America Bulletin*, *121*, 963–978. https://doi.org/10.1130/B26035.1

Jackson, J. A. (1980). Reactivation of basement faults and crustal shortening in orogenic belts. *Nature*, *283*, 343–346.

Jackson, J., & Fitch, T. (1981). Basement faulting and the focal depths of the larger earthquakes in the Zagros mountains (Iran). *Geophysical Journal International*, *64*, 561–586.

Jackson, J., & McKenzie, D. (1984). Active tectonics of the Alpine-Himalayan belt between western Turkey and Pakistan. *Geophysical Journal International*, *77*, 185–264.

Jahani, S., Callot, J., Frizon de Lamotte, D., Letouzey, J., & Leturmy, P. (2007). The Salt Diapirs of the Eastern Fars Province (Zagros, Iran): A brief outline of their past and present, *Thrust Belts and Foreland Basins* (pp. 289–308). Berlin Heidelberg: Springer.

Jahani, S., Callot, J., Letouzey, J., & Frizon de Lamotte, D. (2009). The eastern termination of the Zagros fold-and-thrust belt, Iran: Structures, evolution, and relationships between salt plugs, folding, and faulting. *Tectonics*, *28*, TC6004. https://doi.org/10.1029/2008TC002418

Jahani, S., Hassanpour, J., Mohammadi-Firouz, S., Letouzey, J., de Lamotte, D. F., Alavi, S. A., & Soleimany, B. (2017). Salt tectonics and tear faulting in the central part of the Zagros fold-thrust belt, Iran. *Marine and Petroleum Geology*, *86*, 426–446. https://doi.org/https://doi.org/10.1016/j.marpetgeo.2017.06.003

Jordan, T. H., & Sverdrup, K. A. (1981). Teleseismic location techniques and their application to earthquake clusters in the South-Central Pacific. *Bulletin of the Seismological Society of America*, *71*, 1105–1130.

Karasözen, E., Nissen, E., Bergman, E. A., Johnson, K. L., & Walters, R. J. (2016). Normal faulting in the Simav graben of western Turkey reassessed with calibrated earthquake relocations. *Journal of Geophysical Research: Solid Earth*, *121*, 4553–4574. https://doi.org/10.1002/2016JB012828

Karasözen, E., Nissen, E., Büyükakpınar, P., Cambaz, M., Kahraman, M., Kalkan-Ertan, E., & Özacar, A. (2018). The 2017 July 20 M_w 6.6 Bodrum–Kos earthquake illuminates active faulting in the Gulf of Gökova, SW Turkey. *Geophysical Journal International*, *214*(1), 185–199.

Kennett, B. L. N., Engdahl, E. R., & Buland, R. (1995). Constraints on seismic velocities in the Earth from traveltimes. *Geophysical Journal International*, *122*, 108–124.

Kent, P. E. (1970). The salt plugs of the Persian Gulf Region. *Journal of Petroleum Geology*, *64*, 55–88.

Khadivi, S., Mouthereau, F., Larrasoaña, J. C., Vergés, J., Lacombe, O., Khademi, E., & Suc, J. P. (2010). Magnetochronology of synorogenic Miocene foreland sediments in the Fars arc of the Zagros Folded Belt (SW Iran). *Basin Research*, *22*, 918–932.

Konstantinou, K., & Rontogianni, S. (2011). A comparison of teleseismic and regional seismic moment estimates in the European-Mediterranean region. *Seismological Research Letters*, *82*(2), 189. https://doi.org/10.1785/gssrl.82.2.188

Lohman, R. B., & Simons, M. (2005). Locations of selected small earthquakes in the Zagros mountains. *Geochemistry, Geophysics, Geosystems*, *6*, Q03001. https://doi.org/10.1029/2004GC000849

Maggi, A., Jackson, J. A., Priestley, K., & Baker, C. (2000). A re-assessment of focal depth distributions in southern Iran, the Tien Shan and northern India: Do earthquakes really occur in the continental mantle? *Geophysical Journal International*, *143*, 629–661.

Maggi, A., Priestley, K., & Jackson, J. (2002). Focal depths of moderate and large size earthquakes in Iran. *Journal of Seismology and Earthquake Engineering*, *4*(2–3), 1–10.

Masson, F., Chéry, J., Hatzfeld, D., Martinod, J., Vernant, P., Tavakoli, F., & Ghafory-Ashtiani, M. (2005). Seismic versus aseismic deformation in Iran inferred from earthquakes and geodetic data. *Geophysical Journal International*, *160*, 217–226.

McQuarrie, N. (2004). Crustal scale geometry of the Zagros fold-thrust belt, Iran. *Journal of Structural Geology*, *26*, 519–535.

Molinaro, M., Leturmy, P., Guezou, J. C., Frizon de Lamotte, D., & Eshraghi, S. A. (2005). The structure and kinematics of the south-eastern Zagros fold-thrust belt, Iran: From thin-skinned to thick-skinned tectonics. *Tectonics*, *24*, TC3007. https://doi.org/10.1029/2004TC001633

Morley, C. K., Kongwung, B., Julapour, A. A., Abdolghafourian, M., Hajian, M., Waples, D., & Kazemi, H. (2009). Structural development of a major late Cenozoic basin and transpressional belt in central Iran: The Central Basin in the Qom-Saveh area. *Geosphere*, *5*, 325–362. https://doi.org/10.1130/GES00223.1

Motaghi, K., Shabanian, E., & Kalvandi, F. (2017). Underplating along the northern portion of the Zagros suture zone, Iran. *Geophysical Journal International*, *210*, 375–389. https://doi.org/10.1093/gji/ggx168

Motaghi, K., Shabanian, E., Tatar, M., Cuffaro, M., & Doglioni, C. (2017). The south Zagros suture zone in teleseismic images. *Tectonophys*, *694*, 292–301. https://doi.org/10.1016/j.tecto.2016.11.012

Mouthereau, F., Tensi, J., Bellahsen, N., Lacombe, O., De Boisgrollier, T., & Kargar, S. (2007). Tertiary sequence of deformation in a thin-skinned/thick-skinned collision belt: The Zagros Folded Belt (Fars, Iran). *Tectonics*, *26*, TC5006. https://doi.org/10.1029/2007TC002098

Ni, J., & Barazangi, M. (1986). Seismotectonics of the Zagros continental collision zone and a comparison with the Himalayas. *Journal of Geophysical Research*, *91*, 8205–8218.

Nippress, S., Heyburn, R., & Walters, R. (2017). The 2008 and 2012 Moosiyan earthquake sequences: Rare insights into the role of strike slip and thrust faulting within the Simply Folded Belt (Iran). *Bulletin of the Seismological Society of America*, *107*(4), 1625–1641.

Nissen, E., Emmerson, B., Funning, G. J., Mistrukov, A., Parsons, B., Robinson, D. P., & Wright, T. J. (2007). Combining InSAR and seismology to study the 2003 Siberian Altai earthquakes-dextral strike-slip and anticlockwise rotations in the northern India-Eurasia collision zone. *Geophysical Journal International*, *169*, 216–232.

Nissen, E., Ghods, A., Karasozen, E., Barnhart, W. D., Bergman, E. A., Elliott, J. R., & Talebian, M. (2019). The 12 November 2017 M_w 7.3 Ezgeleh-Sarpol-e Zahab (Iran) earthquake and active tectonics of the Lurestan arc. *Journal of Geophysical Research: Solid Earth*, *124*, 2124–2152. https://doi.org/10.1029/2018JB016221

Nissen, E., Jackson, J., Jahani, S., & Tatar, M. (2014). Zagros "phantom earthquakes" reassessed—The interplay of seismicity and deep salt flow in the Simply Folded Belt? *Journal of Geophysical Research: Solid Earth*, *119*, 3561–3583. https://doi.org/10.1002/2013JB010796

Nissen, E., Tatar, M., Jackson, J. A., & Allen, M. B. (2011). New views on earthquake faulting in the Zagros fold-and-thrust belt of Iran. *Geophysical Journal International*, *186*, 928–944.

Nissen, E., Yamini-Fard, F., Tatar, M., Gholamzadeh, A., Bergman, E., Elliott, J. R., & Parsons, B. (2010). The vertical separation of mainshock rupture and microseismicity at Qeshm island in the Zagros Simply Folded Belt, Iran. *Earth and Planetary Science Letters*, *296*, 181–194.

O'Brien, C. A. E. (1957). Salt diapirism in south Persia. *Geologie en Mijnbouw*, *19*, 357–376.

Oveisi, B., Lavé, J., van der Beek, P., Carcaillet, J., Benedetti, L., & Aubourg, C. (2009). Thick- and thin-skinned deformation rates in the central Zagros simple folded zone (Iran) indicated by displacement of geomorphic surfaces. *Geophysical Journal International*, *176*, 627–654.

Palano, M., Imprescia, P., Agnon, A., & Gresta, S. (2017). An improved evaluation of the seismic/geodetic deformation-rate ratio for the Zagros fold-and-thrust collisional belt. *Geophysical Journal International*, *213*, 194–209. https://doi.org/10.1093/gji/ggx524

Paul, A., Hatzfeld, D., Kaviani, A., Tatar, M., & Péquegnat, C. (2010). Seismic imaging of the lithospheric structure of the Zagros mountain belt (Iran). *Geological Society, London, Special Publications*, *330*, 5–18.

Penney, C., Copley, A., & Oveisi, B. (2015). Subduction tractions and vertical axis rotations in the Zagros-Makran transition zone, SE Iran: the 2013 May 11 M_w 6.1 Minab earthquake. *Geophysical Journal International*, *202*, 1122–1136. https://doi.org/10.1093/gji/ggv202

Ricou, L. E. (1974). *L'étude géologique de la région de Neyriz (Zagros iranien) etl'évolution des Zagrides*, Thesis. Orsay: Université Paris-Sud.

Ricou, L. E., Braud, J., & Brunn, J. H. (1977). Le Zagros. *Mém h. Sér. Soc. Géol. Fr.*, *8*, 33–52.

Roustaei, M., Nissen, E., Abbassi, M., Gholamzadeh, A., Ghorashi, M., Tatar, M., & Parsons, B. (2010). The 25 March 2006 Fin earthquakes (Iran)—Insights into the vertical extents of faulting in the Zagros Simply Folded Belt. *Geophysical Journal International*, *181*, 1275–1291.

Sepehr, M., & Cosgrove, J. W. (2005). Role of the Kazerun Fault Zone in the formation and deformation of the Zagros fold-thrust belt, Iran. *Tectonics*, *24*, TC5005. https://doi.org/10.1029/2004TC001725

Sherkati, S., & Letouzey, J. (2004). Variation of structural style and basin evolution in the central Zagros (Izeh zone and Dezful Embayment), Iran. *Marine and Petroleum Geology*, *21*, 535–554.

Sherkati, S., Letouzey, J., & Frizon de Lamotte, D. (2006). Central Zagros fold-thrust belt (Iran): New insights from seismic data, field observation, and sandbox modeling. *Tectonics*, *25*, TC4007. https://doi.org/10.1029/2004TC001766

Sherkati, S., Molinaro, M., Frizon de Lamotte, D., & Letouzey, J. (2005). Detachment folding in the Central and Eastern Zagros fold-belt (Iran): Salt mobility, multiple detachments and late basement control. *Journal of Structural Geology*, *27*, 1680–1696.

Stöcklin, J. (1968). Structural history and tectonics of Iran: A review. *American Association of Petroleum Geologists Bulletin*, *52*, 1229–1258.

Syracuse, E. M., Phillips, W. S., Maceira, M., & Begnaud, M. L. (2017). Identifying and correcting timing errors at seismic stations in and around Iran, *88*(6), 1472–1479.

Talebian, M., & Jackson, J. (2002). Offset on the main recent fault of NW Iran and implications for the late Cenozoic tectonics of the Arabia-Eurasia collision zone. *Geophysical Journal International*, *150*, 422–439.

Talebian, M., & Jackson, J. (2004). A reappraisal of earthquake focal mechanisms and active shortening in the Zagros mountains of Iran. *Geophysical Journal International*, *156*, 506–526.

Tatar, M., Hatzfeld, D., & Ghafory-Ashtiany, M. (2004). Tectonics of the Central Zagros (Iran) deduced from microearthquake seismicity. *Geophysical Journal International*, *156*, 255–266.

Tatar, M., & Nasrabadi, A. (2013). Crustal thickness variations in the Zagros continental collision zone Iran) from joint inversion of receiver functions and surface wave dispersion. *Journal of Seismology*, *17*(4), 1321–1337.

Tavakoli, F., Walpersdorf, A., Authemayou, C., Nankali, H. R., Hatzfeld, D., Tatar, M., & Cotte, N. (2008). Distribution of the right-lateral strike slip motion from the Main Recent Fault to the Kazerun Fault System (Zagros, Iran): Evidence from present-day GPS velocities. *Earth and Planetary Science Letters*, *275*, 342–347.

Tchalenko, J. S., & Braud, J. (1974). Seismicity and structure of the Zagros (Iran): The Main Recent Fault between 33 and 35° N. *Philosophical Transactions of the Royal Society London*, *277*(1262), 1–25.

Teknik, V., & Ghods, A. (2017). Depth of magnetic basement in Iran based on fractal spectral analysis of aeromagnetic data. *Geophysical Journal International*, *209*, 1878–1891. https://doi.org/10.1093/gji/ggx132

Vergés, J., Emami, H., Garcés, M., Beamud, E., Homke, S., & Skott, P. (2019). Zagros foreland fold belt timing across Lurestan to constrain Arabia–Iran collision. In F. A. Saein (Ed.), *Developments in Structural Geology and Tectonics* (Vol. 3, pp. 29–52). Amsterdam, Netherlands: Elsevier.

Vergés, J., Goodarzi, M. G. H., Emami, H., Karpuz, R., Efstathiou, J., & Gillespie, P. (2011). Multiple detachment folding in Pusht-e Kuh arc, Zagros: Role of mechanical stratigraphy. In K. McClay, J. H. Shaw, & J. Suppe (Eds.), *Thrust fault related folding* (Vol. 94, pp. 69–94). Tulsa, OK: American Association of Petroleum Geologists.

Vergés, J., Saura, E., Casciello, E., Fernàndez, M., Villaseñor, A., Jiménez-Munt, I., & Garcia-Castellanos, D. (2011). Crustal-scale cross-sections across the NW Zagros belt: Implications for the Arabian margin reconstruction. *Geological Magazine*, *148*, 739–761.

Vernant, P., Nilforoushan, F., Hatzfeld, D., Abbassi, M. R., Vigny, C., Masson, F., & Chéry, J. (2004). Present-day crustal deformation and plate kinematics in the Middle East constrained by GPS measurements in Iran and northern Oman. *Geophysical Journal International*, *157*, 381–398.

Walker, R. T., Andalibi, M. J., Gheitanchi, M. R., Jackson, J. A., Karegar, S., & Priestley, K. (2005). Seismological and field observations from the 1990 November 6 Furg (Hormozgan) earthquake: A rare case of surface rupture in the Zagros mountains of Iran. *Geophysical Journal International*, *163*, 567–579.

Walker, R. T., Bergman, E. A., Szeliga, W., & Fielding, E. J. (2011). Insights into the 1968–1997 Dasht-e-Bayaz and Zirkuh earthquake sequences, eastern Iran, from calibrated relocations, InSAR and high-resolution satellite imagery. *Geophysical Journal International*, *187*, 1577–1603.

Walker, R., & Jackson, J. (2004). Active tectonics and late Cenozoic strain distribution in central and eastern Iran. *Tectonics*, *23*, TC5010. https://doi.org/10.1029/2003TC001529

Walpersdorf, A., Hatzfeld, D., Nankali, H., Tavakoli, F., Nilforoushan, F., Tatar, M., & Masson, F. (2006). Difference in the GPS deformation pattern of North and Central Zagros (Iran). *Geophysical Journal International*, *167*, 1077–1088.

Wessel, P., Smith, W. H. F., Scharroo, R., Luis, J., & Wobbe, F. (2013). Generic mapping tools: Improved version released. *Eos, Transactions American Geophysical Union*, *94*, 409–410.

Weston, J., Ferreira, A. M. G., & Funning, G. J. (2011). Global compilation of interferometric synthetic aperture radar earthquake source models: 1. Comparisons with seismic catalogs. *Journal of Geophysical Research*, *116*, B08408. https://doi.org/10.1029/2010JB008131

Yamini-Fard, F., Tatar, M., Hessami, K., Gholamzadeh, A., & Bergman, E. A. (2012). Aftershock analysis of the 2005 November 27 (M_w 5.8) Qeshm Island earthquake (Zagros-Iran): Triggering of strike-slip faults at the basement. *Journal of Geodynamics*, *61*, 138–147.